ADT-1004: A First-in-Class, Orally Bioavailable Selective pan-RAS Inhibitor for Pancreatic Ductal Adenocarcinoma

Dhana Sekhar Reddy Bandi[1], Ganji Purnachandra Nagaraju[1], Sujith Sarvesh[1], Julienne L. Carstens[1], Jeremy B. Foote[2], Emily C. Graff[3], Yu-Hua D Fang[4], Adam B. Keeton[5,12], Xi Chen[5,12], Kristy L. Berry[4], Sejong Bae[6], Mehmet Akce[1], Greg Gorman[7], Karina J. Yoon[8], Upender Manne[9], Micheal R. Boyd[12], Donald J. Buchsbaum[10], Asfar S. Azmi[11], Yulia Y. Maxuitenko[5], Gary A. Piazza[5,12], Bassel F. El-Rayes[1*]

[1]Department of Hematology and Oncology, University of Alabama at Birmingham, Birmingham, AL-35233, USA; [2]Department of Microbiology, University of Alabama at Birmingham, Birmingham, AL-35233, USA; [3] Department of Pathobiology, College of Veterinary Medicine, Auburn University, Auburn, AL-36849. [4]Radiology and Neurology, University of Alabama at Birmingham, Birmingham, AL-35233, USA; [5]Drug Discovery and Development Department, Harrison College of Pharmacy, Auburn University, Auburn, AL-36849, USA; [6]Division of Preventive Medicine, University of Alabama School of Medicine, Birmingham, AL-35233, USA; [7]Department of Pharmaceutical, Social and Administrative Sciences, Samford University, Birmingham, AL-35229, USA; [8]Department of Pharmacology and Toxicology, University of Alabama at Birmingham, Birmingham, AL-35233, USA; [9]Department of Pathology, University of Alabama at Birmingham, Birmingham, AL-35233, USA; [10]Department of Obestetrics and Gynecology, University of Alabama at Birmingham, Birmingham, Alabama, Birmingham, AL-35233, USA; [11]Department of Oncology, Karmanos Cancer Institute, Wayne State University School of Medicine, Detroit, MI-48201, USA; [12]ADT Pharmaceuticals, LLC, Orange Beach, AL-31691, USA.

***Corresponding Author: Bassel F. El-Rayes, MD** Albert F. LoBuglio Endowed Chair for Translational Cancer Research, Division Director, Hematology and Oncology, Deputy Director, O'Neal Comprehensive Cancer Center, Heersink School of Medicine, University of Alabama at Birmingham. **belrayes@uabmc.edu**

Running title: Novel pan-RAS Selective Inhibitor for Pancreatic Cancer

Disclosure of Potential Conflicts of Interest: G.A. Piazza, A.B. Keeton, X. Chen, and M.R. Boyd are co-founders of ADT Pharmaceuticals Inc. and consultants. All other authors declare no potential conflicts of interest.

Funding Sources: NIH/NCI R01CA254197, R01CA238514, and P30CA01314

ABSTRACT:

Here, we evaluated *in vivo* antitumor activity, target engagement, selectivity, and tumor specificity of ADT-1004, an orally bioavailable prodrug of ADT-007 having highly potent and selective pan-RAS inhibitory activity. ADT-1004 strongly blocked tumor growth and RAS activation in mouse PDAC models without discernable toxicity. As evidence of target engagement and tumor specificity, ADT-1004 inhibited activated RAS and ERK phosphorylation in PDAC tumors at dosages approximately 10-fold below the maximum tolerated dose and without discernable toxicity. ADT-1004 inhibited ERK phosphorylation in PDAC tumors. In addition, ADT-1004 blocked tumor growth and ERK phosphorylation in PDX PDAC models with $KRAS^{G12D}$, $KRAS^{G12V}$, $KRAS^{G12C}$, or $KRAS^{G13Q}$ mutations. ADT-1004 treatment increased $CD4^+$ and $CD8^+$ T cells in the TME consistent with exhaustion and increased $MHCII^+$ M1 macrophage and dendritic cells. ADT-1004 demonstrated superior efficacy over sotorasib and adagrasib in tumor models involving human PDAC cells resistant to these $KRAS^{G12C}$ inhibitors. As evidence of selectivity for tumors from PDAC cells with mutant KRAS, ADT-1004 did not impact the growth of tumors from RAS^{WT} PDAC cells. Displaying broad antitumor activity in multiple mouse models of PDAC, along with target engagement and selectivity at dosages that were well tolerated, ADT-1004 warrants further development.

Significance: ADT-1004 displayed robust antitumor activity in aggressive and clinically relevant PDAC models with unique tumor specificity to block RAS activation and MAPK signaling in RAS mutant cells. As a pan-RAS inhibitor, ADT-1004 has broad activity and potential efficacy advantages over allele-specific KRAS inhibitors by averting resistance. These findings support clinical trials of ADT-1004 for KRAS mutant PDAC.

Keywords: Pancreatic ductal adenocarcinoma, pan-RAS inhibitor, tumor immune microenvironment, KRAS, RAS-driven malignancies

Introduction

Pancreatic ductal adenocarcinoma (PDAC) is projected to become the second leading cause of cancer deaths in the US by 2040.[1, 2] In 2024, PDAC is expected to cause 52,580 deaths in the US.[3] Systemic treatment strategies for PDAC have yielded little improvement in survival.[4] The overall survival rate at 5-years remains at 12% for patients diagnosed at early stages or 3% for those diagnosed with metastatic disease.[5] Hence, developing novel systemic treatment strategies is essential for improving the survival of patients with PDAC.

The gene encoding for KRAS, a small GTPase protein, is mutated in more than 90% of PDAC patients. KRAS mutations in patients with PDAC include G12D (37.0%), G12V (28.2%), G12R (12.7%), G12C (2.7%), or others (7.0%), and some have multiple mutations in RAS (2.1%).[6,7,8] The National Cancer Institute has identified anti-KRAS testing as one of four essential components for PDAC drug screening and development.[9,10] Targeting this oncoprotein has proven challenging because it lacks a relatively flat surface for suitable small molecule binding sites.[11] To date, the U.S. Food and Drug Administration (FDA) has approved two $KRAS^{G12C}$ inhibitors, sotorasib (AMG-510) and adagrasib (MRTX849) for treatment of lung cancer. Several newer inhibitors targeting different KRAS mutations are in preclinical development or clinical trials. Sotorasib and adagrasib have limited use in PDAC, given that $KRAS^{G12C}$ is mutated in less than 3% of patients diagnosed with PDAC.[12] The development of adaptive resistance also limits the efficacy $KRAS^{G12C}$ inhibitors in patients diagnosed with $KRAS^{G12C}$ mutant cancers.[13] Resistance mechanisms include new KRAS mutations or activation of RAS^{WT} isozymes (HRAS and NRAS) from upstream receptor tyrosine kinases.[14] Consequently, a pan-RAS inhibitor could provide a more effective approach to address the complex mutational landscape of PDAC that can escape compensatory mechanisms contributing to intrinsic or adaptive resistance.

To address these limitations, we developed and recently characterized ADT-007, a highly potent and selective pan-RAS inhibitor with broad activity against a histologically diverse range of RAS-mutant cancer cell lines.[15] ADT-1004 is an orally bioavailable prodrug of ADT-007 designed to improve the water solubility and metabolic stability of ADT-007 (**Figure 1A**). This study evaluated the antitumor activity and target selectivity of ADT-1004 in aggressive and clinically relevant mouse and PDX models of PDAC. We also defined various pharmacological

94 attributes of ADT-1004 that could set this drug candidate apart from other KRAS inhibitors
95 approved or in development.
96
97 **Materials and methods**
98 ***Synthesis of ADT-1004***

99 Synthesis of ADT-1004 HCl [(Z)-4-((5-fluoro-3-(2-((furan-2-ylmethyl)amino)-2-oxoethyl)-2-
100 methyl-1H-inden-1-ylidene)methyl)-2,6-dimethoxyphenyl (1-methylpiperidin-4-yl)carbamate
101 hydrogen chloride]: To a solution of 1-methylpiperidin-4-amine (2.3 g, 20 mmol) in dry
102 chloroform (40 mL, freshly distilled from P_2O_5), triphosgene (2.2 g, 7 mmol) was added in
103 portion with stirring, followed by addition of triethylamine (7 mL). The reaction mixture was
104 refluxed for 6h. (Z)-2-(5-fluoro-1-(4-hydroxy-3,5-dimethoxybenzylidene)-2-methyl-1H-inden-3-
105 yl)-N-(furan-2-ylmethyl) acetamide (ADT-007, synthesis was previously described [15]) (3.0 g, 6.7
106 mmol) and dibutyltin dilaurate (7.4 g, 11.6 mmol) were added and the mixture synthesized from
107 the reaction was stirred at 65 °C overnight. The solvents were extracted under vacuum and silica
108 gel column chromatography was used to purify the residue, followed by the addition of 1.00 eq.
109 of HCl (1N in dioxane, 0 °C) to yield ADT-1004 HCl as a yellow crystal (yield was 55%).

110 ***Cell lines***

111 The human PDAC cell lines, MIA PaCa-2 and BxPc-3, were acquired from the American Type
112 Culture Collection (ATCC; Manassas, VA, USA) and cultured under the manufacturer's
113 provided guidelines. 2838c3 mouse PDAC cells were purchased from Kerafast (Boston, MA,
114 USA), and the KPC cell line was gifted by Dr. Gregory Lesinski (Emory University, USA). MIA
115 PaCa-2 cells resistant to $KRAS^{G12C}$-inhibitors (MIA-AMG-Res) were generated by us as
116 previously described.[16] All cells were grown in a humidified atmosphere at 37 °C with 5% CO_2,
117 utilizing either Dulbecco's Modified Eagle Medium (DMEM, ATCC, #30-2002) for 2838c3 or
118 Roswell Park Memorial Institute (RPMI)-1640 Medium (ATCC, #30-2001) for BxPc3 with 10%
119 fetal bovine serum (FBS, ATCC, #30-2020) and 1% penicillin/streptomycin (ATCC, #30-2101)
120 in common. Furthermore, MIA PaCa-2 cells received an additional supplementation of 1% horse
121 serum (Gibco, #16050-122) in DMEM along with 10% FBS and 1% penicillin/streptomycin. All
122 cell lines were routinely tested for mycoplasma and other pathogen contaminations.
123 ***Cell growth assays***

124 MIA PaCa-2 and MIA-AMG-Res were plated in 96-well culture plates at a density of 4×10^3 cells
125 per well. After overnight incubation, the cells were treated with ADT-007, sotorasib, or
126 adagrasib (Selleckchem, Houston, TX, USA). After 72 h, 10 µl methylthiazole tetrazolium
127 (MTT; 5 mg/mL in PBS; Sigma-Aldrich) was added, and the cells were incubated for another 2 h
128 at 37 °C. The resulting formazan crystals were solubilized in 100 µl DMSO and mixed well by
129 pipetting, and absorbance was measured at 570 nm and 630 nm using the Biotek Synergy MX
130 Multi Format Microplate Reader. The average measurement at 630 nm was subtracted from the
131 average at 590 nm, and relative growth rate was plotted with respect to control-treated cells.

132 ***Clonogenic assays***

133 At a density of 1000 cells per well in 6-well plates, MIA PaCa-2 and MIA-AMG-Res cells were
134 seeded and exposed to ADT-007, sotorasib, or adagrasib for 72 h. Following the treatment, the
135 medium containing the drug was replaced with fresh medium, and the plates were then placed in
136 a CO_2 incubator for 1 week (for MIA-AMG-Res colonies) or 10 days (for MIA PaCa-2
137 colonies). After the incubation period, the medium was removed, and colonies were fixed using
138 methanol, followed by crystal violet staining for 15 min. The colonies were photographed after a
139 thorough wash and drying process.

140 ***Immunoblot analysis***

141 Tumor tissues were lysed in RIPA buffer (Thermo Scientific, #89901) and protein concentrations
142 assayed using a bicinchoninic acid (BCA) protein assay (Thermo Fisher Scientific, #23225). 40
143 µg of protein lysate was separated through 4-20% SDS-PAGE (BIO-RAD, #4568096) and
144 transferred onto PVDF membranes (Invitrogen, #IB34001). The membranes were then incubated
145 with antibodies diluted in 2% Bovine Serum Albumin (BSA, Fisher Scientific, #BP1600) for 2 h
146 at room temperature. Primary antibodies were phospho ERK (Cell Signaling Technology #9121;
147 1:1000), total ERK (Cell Signaling Technology (CST) #9122; 1:1000), anti-beta actin (Santa
148 Cruz #sc-47724; 1:3,000). Incubation with HRP-linked secondary antibodies (CST,
149 #7074/7076;) at a dilution of 1:3000 in a 2% BSA solution was carried out for 1 h at room
150 temperature. The signal was then detected on the LI-COR Odyssey DLx Imager using the ECL
151 chemiluminescence detection system (Thermo Fisher Scientific, #34577).

152 ***Active RAS detection assay***

153 RAS activation (RAS-GTP) levels were measured using the Cell Signaling Technology RAS
154 activation assay kit (#8821). Lysates were prepared from tumors collected from ADT-1004 or
155 vehicle treated mice by performing the steps provided by the manufacturer protocol. Briefly,
156 tumors were lysed using the provided lysis buffer supplemented with protease and phosphatase
157 inhibitors. A total of 1 mg/mL lysate in 1X lysis buffer was employed for the experiment. Equal
158 amounts of protein were then incubated with the GST-Raf1-RBD protein, and the reaction
159 mixture was loaded onto a RAS affinity resin to capture activated RAS. Following extensive
160 washing to remove unbound proteins, the activated RAS was eluted in sample buffer and
161 subjected to immunoblotting using Ras Mouse mAb (1:200 dilution) with gentle agitation
162 overnight at 4 °C. The membrane was then probed with anti-mouse IgG, HRP-linked antibody
163 (1:2000, #7076), and HRP-conjugated anti-biotin antibody (1:1000, #7075) to detect biotinylated
164 protein markers. The signal was detected using chemiluminescent reagents, and the resulting
165 bands were quantified using an imaging system.

166 **Pharmacokinetic study**

167 Following acclimatization in the Biologic Research Laboratory at the University of South
168 Alabama, College of Medicine 6-8-week-old female C57BL/6 mice (Envigo, strain 044) were
169 randomly assigned to two groups (n=4) and received ADT-1004 (100 mg/kg, in water) by oral
170 gavage once. Blood was drawn at 1, 2, 4, or 8 h (each animal was bled twice) into K_2EDTA-
171 microtainer tubes followed by separation of plasma. ADT-1004 levels in plasma as well as ADT-
172 007 levels generated following oral administration of ADT-1004 were determined using reverse
173 phase chromatography with MS/MS detection. The study followed established guidelines and
174 adhered to the approved protocol of the University of South Alabama Institutional Animal Care
175 and Use Committee (IACUC).

176 **Maximum tolerated dose (MTD) study**

177 Following acclimatization in Biological Research Facility at Auburn University 7-8-week-old
178 female C57BL/6 mice (Charles River Laboratories, stain 027) which were subcutaneously
179 implanted with mouse 2838c3 PDAC cells (1×10^6 cells resuspended in 100 µL PBS), were
180 randomly assigned to groups and received either vehicle (citric acid with sodium citrate
181 monobasic in water, n=10) or ADT-1004 (125-225 mg/kg, n=5/dose) by oral gavage twice daily
182 (BID), five days a week (5x/week) for 3.5 weeks. Mice were observed for adverse reaction to the

183 treatment daily and tumor measurements and body weights were monitored biweekly. At the end
184 of the study (a total of 18 daily treatments), mice in the group treated with MTD of ADT-1004
185 (defined as a dose that produced no deaths and no more than 5% body weight loss) were
186 euthanized, and blood was collected and submitted for clinical chemistries and complete blood
187 counts to the Auburn University Clinical Pathology Laboratory. Mice were necropsied, organs
188 were collected and fixed for histopathological analysis, and bone marrow smears were prepared
189 for cytology. Blinded assessment of organ viscera (heart, lung, kidney, liver, stomach, pancreas,
190 duodenum, jejunum, ileum, cecum, and colon) was performed following standard procedures by
191 board-certified veterinary pathologists. The MTD study followed established guidelines and
192 adhered to the approved protocol of the Auburn University IACUC.

193 **Mouse tumor xenograft experiments**

194 *PDAC (MIA PaCa-2, MIA-AMG-Res, and BxPc-3) cell-derived tumor xenograft models*

195 Following acclimatization in the University of Alabama at Birminghamn (UAB) animal housing
196 facility, male NSG (NOD.Cg-Prkdc^{scid} Il2^{rgtm1Wjl}/SzJ) mice aged 4 to 5 weeks (stock no. 005557;
197 the Jackson Laboratory) were subcutaneously implanted with MIA PaCa-2, *MIA-AMG-Res*, or
198 BxPc3 PDAC cells. A total of 1×10^6 cells (for MIA PaCa-2 and *MIA-AMG-Res*) and 5×10^6
199 cells (BxPc-3), resuspended in 200 µL PBS, were unilaterally injected into the right flank of
200 mice using a BD 26Gx 5/8 1 mL Sub-Q syringe. Seven days post-transplantation or when tumors
201 reached approximately 80–100 mm^3 in size, recipient mice were randomly assigned to 4 groups
202 (n=5) and received either vehicle, ADT-1004 (40 mg/kg), sotorasib (40 mg/kg), or adagrasib (40
203 mg/kg) through oral gavage. For BxPc3-implanted mice, two groups were established (n=5), and
204 mice were orally administered either vehicle or ADT-1004 (40 mg/kg). Tumor volumes and
205 body weights were monitored biweekly, with the formula to calculate the tumor volume as
206 length × width^2 × 0.5. After completing the drug dosing regimen, tumors from vehicle and
207 treatment groups were utilized for molecular analysis. *In vivo* studies followed established
208 guidelines and adhered to the approved protocol of the UAB Institutional Animal Care and Use
209 Committee (IACUC).

210 *Orthotopic pancreatic injection of murine PDAC cells (KPC and 2838c3)*

211 C57BL6/J mice (stock no. 000664; The Jackson Laboratory) were subjected to isoflurane
212 anesthesia, followed by an intra-abdominal incision to access the spleen and pancreas. A
213 Matrigel suspension (40 μL), containing either KPC-*f* -luc or 2838c3- *f* -luc cells (1×10^5), was
214 injected into the tail of the pancreas. The skin and abdominal wall were then closed by suturing.
215 Following a week, mice were divided into treatment groups at random (n=5-7 per group) and
216 given oral dosages once daily (QD), 5 days/week of vehicle (citric acid with sodium citrate
217 monobasic) or ADT-1004 (40 mg/kg) until completing the experiment. Imaging sessions
218 involving D-luciferin injection were conducted bi-weekly throughout the study. The total
219 luminescence from tumor-bearing regions was quantified using the Living image *in vivo* imaging
220 software. No indications of toxicity, such as changes in body weight or abnormalities in organs,
221 were observed. At the endpoint, mice were euthanized, and their tumors were harvested and
222 weighed for analysis.

223 ***Flow cytometry***

224 Tumors derived from 2838c3-*f*-luc and KPC-*f*-luc PDAC cells implanted into the pancreas of
225 C57BL6/J mice were subjected to digestion using a solution comprising 0.1 mg/ml DNase 1 and
226 1 mg/ml collagenase IV (Worthington Biochemical, Lakewood, NJ) in Hank's Balanced Salt
227 Solution (HBSS) at 37 °C with shaking, for 45 min. Following digestion, the samples underwent
228 rinsing with RPMI-1640 supplemented with 10% FBS, and a 70 μm strainer was used to filter
229 them to produce single-cell suspensions. The separated cells were labeled for 30 to 60 min at 4
230 °C using primary antibodies coupled to fluorophores and a live/dead dye (**Supplementary Table**
231 **1**). Cells were then rinsed and suspended in a flow buffer. After labeling the cell surface, the
232 cells were fixed at 4 °C in 4% paraformaldehyde or FoxP3 transcription buffer set (eBioscience;
233 # 00-5523-00) for 45 min and then washed with 1x Perm/Wash (BD, 554723). Data acquisition
234 was conducted using a Symphony A5 flow cytometer, and analysis was performed using FlowJo
235 version 10.7.2.

236 **KRAS –mutant patient-derived tumor xenograft studies**

237 *Mouse tumorigenesis experiments using PDAC PDX models*

238 Mouse experiments were conducted using PDAC PDX models with distinct KRAS mutations
239 G12D and G12C (generously provided by Dr. Karina Yoon), [17] G12V and G13Q (obtained from

240 Dr. Upendar Manne). Male NSG mice (5–6 weeks old, stock no. 005557; the Jackson
241 Laboratory) were utilized for the experiments. In brief, F1 generation tumors were cut into 2-
242 mm × 2-mm fragments and subcutaneously implanted by way of a small incision produced in the
243 right flanks of NSG mice while they were anesthetized. Tumor size and body weights were
244 monitored biweekly. Tumor volume was calculated using the formula: length × width^{2} × 0.5.
245 Once tumors reached approximately 80–100 mm^{3}, mice (n=6 per group) were randomly
246 assigned to receive daily oral doses of either vehicle (citric acid with sodium citrate monobasic)
247 or the pan-RAS inhibitor ADT-1004 (40 mg/kg) until the conclusion of the experimental period.
248 At the study's end, mice were euthanized, and tumor images and weights were documented. The
249 UAB's IACUC approved the experimental protocol for these mouse studies.

250 ***Immunohistochemical Staining and Evaluation***

251 Animal tumor tissues were fixed in 10% formalin for 24 h, dehydrated, paraffin
252 embedded, and sectioned with 5µM thickness for immunohistochemistry. Antigen retrieval was
253 performed from the sectioned slides by using 10 mM citrate buffer, pH 6.0 for 5 min
254 (microwave) for all the antibodies used (phospho-ERK, α-SMA, and Ki67). The slides were then
255 rinsed with PBS followed by blocking with 5% BSA for 30 min. The sections were then probed
256 with the primary antibodies overnight at 4 °C as follows: αSMA (Abcam, #ab7817, 1:500),
257 phospho-ERK (CST, #4370, 1:500), and Ki-67 (CST, #9449 1:500). Following the antibody
258 incubation, the slides were washed and incubated for 30 min with biotinylated anti-mouse/rabbit
259 IgG secondary antibody. Afterwards, the slides were washed and incubated with VectaStain Elite
260 ABC reagent (Vector Laboratories, #PK-8200) for 30 min and the counterstaining was
261 performed for 1 min with hematoxylin reagent (Sigma-Aldrich, #51275), followed by washing
262 and mounting with mounting medium (epredia, #4112). Stained slides were imaged using the
263 Echo Revolution automated microscope (ECHO, USA) at 20× magnification, and quantified
264 using ImageJ with the same threshold for each stain and the results are shown as percent staining
265 per visual field.

266 **Multiplex Immunofluorescence**

267 *Hyperplex staining and whole-slide imaging*

268 FFPE (formalin fixed, paraffin embedded) slides containing vehicle and ADT-1004 treated
269 TMAs (Tumor microarrays)were processed using Biogenex EZ Retriever system and EZ-AR2
270 Elegance (#HK546-XAK) at 107 °C for 15 min. Cyclical multiplex immunofluorescence was

271 then performed using the Lunaphore COMET seqIF staining platform at the UAB Flow
272 Cytometry and Single Cell core facility. In brief, all primary antibodies were diluted in multi-
273 staining buffer (BU06, Lunaphore) **Table S1** and incubated for 4 min. Secondary antibodies
274 diluted in antibody diluent (LI-COR # 927-65001) **Table S1** and DAPI counterstain were
275 incubated for 2 min. Imaging was performed using an image buffer (BU09, Lunaphore) for the
276 following exposure times: DAPI 80 ms, TRICTC 400 ms, and Cy5 200 ms. Elution after each
277 cycle was performed for 2 min at 37 ^{0}C in the elution buffer (BU07-L, Lunaphore) followed by a
278 30 sec quenching step with quenching buffer (BU08-L, Lunaphore). Upon completion of the
279 experiment, an aligned, stitched, flat-field corrected 16-bit OME-TIFF image file was generated
280 for each slide. Images were pre-processed to subtract autofluorescence from each channel using
281 Lunaphore Horizon Viewer and exported for further analysis.

282 **Image Segmentation and Quantification**

283 Visiopharm Oncotopix Image Analysis suite was used to de-array the whole slide scans (allows
284 the retention of each TMA core as an individual biological replicate), tissue regions hand
285 selected to remove artifacts such as folds and debris, identify sub-tissue region of interests
286 (epithelium vs other based on Keratin 17-19 stain thresholds), and cell segmentation (based on
287 Nuclear Segmentation AI, Deep Learning app with Keratin 17-19, CD3, CD11b and PDGFRb
288 stains for membrane boundaries). Cellular phenotyping was performed using the change by
289 intensity post-processing tool output in an app for known marker populations in a stepwise
290 fashion with the undefined cell population resulting in the following populations being also
291 negative for the previous markers: Cancer –Epithelium (Ker17/19 high), Cancer dim (Ker 17/19
292 dim), B cells (Ker-17/19-CD19^{+}), T cells (Ker-17/19-CD19-CD3^{+}), Cytotoxic T cells (Ker-
293 17/19-CD19-CD3^{+}CD8^{+}), T effector (Ker-17/19-CD19-CD3^{+} CD4^{+}), T regulatory (Ker-17/19-
294 CD19-CD3^{+}CD4^{+}Foxp3^{+} and Ker-17/19-CD19-CD3^{+}Foxp3^{+} if CD4 membranous stain was
295 outside of the sectioning plane), macrophages (Ker-17/19-CD19-CD3-CD11b^{+}), neutrophils
296 (Ker-17/19-CD19-CD3-CD11b-Ly6G^{+}), myeloid derived suppressor cells (Ker-17/19-CD19-
297 CD3-CD11b-CD11b^{+}Ly6G^{+}), endothelial (Ker-17/19-CD19-CD3-CD11b-CD11b-Ly6G-
298 CD31^{+}), and cancer associated fibroblasts (negative for all other markers and positive for any of
299 the mesenchymal markers: αSMA, FAP, PDGFRβ, desmin and integrinβ3). Expression of
300 functional markers whose expression was of interest regardless of cellular population (pAKT,
301 pERK, CD11b, αSMA, FAP, PDGFRβ, Desmin and Integrinβ3) was exported using the

302 phenoplex guided workflow. Cellular features such as phenotype, marker positivity, x, y
303 coordinates, area, and shapes (form factor and ellipticalness) were exported for each cell. Count
304 analyses and percentages were calculated in xcel using pivot tables and graphed in Prism.

305 **Spatial Analysis**

306 Cell-cell infiltration was calculated using the G-Function for each pairwise target and neighbor
307 analysis every 10um radii for 10-200um for each TMA core. Vehicle and ADT-1004 treated
308 tumor cores were averaged and significant differences at each radii point were calculated using a
309 t-test.

310 Marker expression analysis of interesting co-localization phenotypes were calculated using a
311 MATLAB script delineated as follows:

312 For cells type X, type Y and marker A

313 Under a given radius r, assume that we can find:

314 X1 cells for cells that are: X type, expressing A, and has at least one Y cell within r

315 X2 cells for cells that are: X type, not expressing A, and has at least one Y cell within r

316 X3 cells for cells that are: X type, expressing A, and has no Y cells within r

317 X4 cells for cells that are: X type, not expressing A, and has no Y cells within r

318 X5 cells that are: X type, has at least one A-positive Y cell within r

319 X6 cells that are: X type, has at least one A-negative Y cell within r

320 X7 cells that are: X type, no A-positive Y cells within r

321 X8 cells that are: X type, no A-negative Y cells within r

322 X9 cells for cells that are: X type, has at least one Y cell within r (total number of X co-
323 localization with Y)

324 Sum of X1~X4 will be the total number of X cells. X1+X3 will be the total number of A-
325 expressing X cells. X1+X2 will be the total number of X cells with co-localization with r.
326 X5+X7 = X6+X8 = X = total number of X.

327 We then define:

328 M1 = X1/(X1+X2). M1 is the fraction of A-expression in X that co-localize with Y

329 M2 = X3/(X3+X4). M2 is the fraction of A-expression in X that do not colocalize with Y

330 M3 = X1/(X1+X3). M3 is the fraction of co-localization of X with Y out of all A-
331 expressing X cells

M4 = X2/(X2+X4). M4 is the fraction of colocalized X cells out of all non-A-expressing X cells

M5 = X5/X. M5 is the fraction of X that co-localizes with A-positive Y

M6 = X6/X. M6 is the fraction of X that co-localizes with A-negative Y.

Statistical Analyses

Statistical analyses and data visualization were done using GraphPad Prism (version 9.1.2). The data are represented as means accompanied by either standard deviation (SD) or standard error of the mean (SEM). A repeated measures analysis of variance (ANOVA) or ANOVA with Bonferroni correction and a two-tailed Student's t-test were conducted to evaluate and apply multiple corrections for assessing statistical significance between groups. To determine IC_{50} values, concentrations were log-transformed, and the data were normalized to the control, followed by a log (inhibitor) vs. response (four-parameter nonlinear dose-response) analysis. A statistical significance threshold was set at $p < 0.05$.

346 **Results**

347 **ADT-1004 inhibits tumor growth in murine models of PDAC**

348 Initial experiments were conducted to confirm oral bioavailability and sufficient
349 conversion of the prodrug, ADT-1004, to it active metaobolite, ADT-007 *in vivo*. Following
350 administration of a single oral dose of 100 mg/kg ADT-1004 generated sustained plasma levels
351 of ADT-007 for at least 8 h that were appreciably higher than growth IC_{50} values (**Figure 1B**).
352 Next, the maximum tolerated dose (MTD) of ADT-1004 was established when administered by
353 oral gavage BID, 5x/week for 3.5 weeks using tumor-bearing mice. The results revealed no
354 significant differences in body weight between the vehicle and ADT-1004 treated groups at
355 dosages up to 175 mg/kg BID (**Figure 1C**). Dosages above 175 mg/kg BID resulted in
356 significant weight loss (data not shown). Blinded analysis of H&E stained tissues from mice
357 treated with 175 mg/kg BID ADT-1004 confirmed no discernable histopathologic abnormalities
358 in the heart, lungs, kidneys, liver, jejunum, pancreas, and colon (**Figure 1D**). In addition,
359 analysis of clinical chemistries, complete blood counts, and bone marrow cytology revealed no
360 significant differences in markers of liver and renal function, electrolytes, energy metabolism,
361 and hematologic function between mice treated with vehicle or ADT-1004 at the 175 mg/kg BID
362 dose (**Supplementary Figure 1**).

363 To determine antitumor activity of ADT-1004, luciferase-labeled KPC (KPC-Luc) cells
364 with point mutations in $KRAS^{G12D}$ and $p53^{R172H}$ were surgically implanted into the pancreas of
365 C57BL6/J mice and imaged one week after implantation (day 0) to randomize mice between the
366 control (vehicle) and ADT-1004 treatment groups. Treatment was started on day 0 by once daily
367 oral gavage with either vehicle or ADT-1004 at dosages ranging from 10 – 50 mg/kg (5x/week)
368 **(Figure 1E)**. Mice were euthanized on day 27 to determine treatment effects on tumor growth by
369 measuring bioluminescence and tumor weight (**Figure 1F**). Most mice in the ADT-1004
370 treatment groups displayed reduced bioluminescence compared with mice treated with vehicle.
371 Doses of ADT-1004 from 20-50 mg/kg demonstrated comparable statistically significant
372 reductions in tumor weights compared to vehicle-treated mice (**Figure 1F**) with no significant
373 differences in body weight between the treated and vehicle groups (**Figure 1G**). Measurement
374 of ADT-1004 and ADT-007 levels in plasma by LC-MS/MS from ADT-1004 treated mice
375 revealed that the 40 mg/kg dose generated comparable levels as a 50 mg/kg dosage (**Figure 1H**

376 and **1I**). We therefore selected 40 mg/kg dose for further investigation as this dose appeared to
377 be the lowest possible dose that could achieve maximum systemic levels of ADT-007.

378 **Tumor growth inhibition by ADT-1004 is associated with reduced activated RAS and**
379 **pERK levels**

380 The mechanism responsible for the anti-cancer activity of ADT-007 was previously
381 reported to involve direct binding to RAS within the nucleotide-binding domain to block GTP
382 activation of RAS and suppress effector interactions and downstream MAPK/AKT signaling.[15]
383 We therefore conducted a second experiment using the KPC orthotopic model (with $KRAS^{G12D}$
384 mutation) described above to confirm that ADT-1004, as a prodrug of ADT-007, inhibits tumor
385 growth by blocking RAS activation. Similar to results from the first experiment, oral
386 administration of ADT-1004 at a dosage of 40 mg/kg demonstrated a significant reduction in
387 tumor growth compared with the vehicle group, as evidenced by the bioluminescence imaging
388 and tumor weight without differences in body weight (**Figure 2A-E**). The tumor tissues were
389 analyzed for immune changes using multi-parameter flowcytometry to identify myeloid, T, NK,
390 and tumor cells in the TME (**Supplemental Figure 8**). Consistent with *in vitro* studies of ADT-
391 007,[15] measurement of activated RAS levels by RAS-RBD pull-down assays showed that tumors
392 from ADT-1004 treated mice had significantly reduced RAS-GTP levels compared with tumors
393 from vehicle-treated mice (**Figure 2G**). Tumors from mice treated with ADT-1004 treatment
394 group also showed reduced pERK levels compared with tumors from the vehicle group (**Figure**
395 **2H**).

396 Next, we determined the antitumor activity of ADT-1004 in additional mouse PDAC
397 models. First, we employed a different syngeneic, immunocompetent orthotopic mouse model in
398 which 2838c3-luc cells were implanted into the pancreas of female C57BL6/J mice (**Figure 3A**).
399 Mice were treated 5x/week with either vehicle or ADT-1004 at 20 mg/kg QD, 20 mg/kg BID, or
400 40 mg/kg QD. Measurement of bioluminescence and tumor weights showed that all three ADT-
401 1004 dose groups displayed comparable significantly reduced tumor size compared with the
402 vehicle group with no significant differences in body weight (**Figure 3A-E**).

403 We also determined if the antitumor activity of ADT-1004 in the 2838c3 orthotopic
404 PDAC model was associated with reduced levels of activated RAS. Similar to results in the KPC
405 orthotopic model, RAS-RBD pull-down assays showed a significant reduction of RAS-GTP
406 levels in tumors from ADT-1004-treated mice compared with tumors from vehicle-treated mice

407 (**Figure 3F**). A notable decrease in the pERK levels was also observed in mice treated with
408 ADT-1004 at 40 mg/kg, providing additional evidence that the antitumor activity of ADT-1004
409 is mediated by inhibition of activated RAS (**Figure 3G**) and consistent with previous *in vitro*
410 studies of ADT-007.[15]

411 **ADT-1004 alters tumor immune microenvironment (TiME) by inhibiting KRAS^{G12D}**

412 Considering the growing literature reporting that mutation-specific KRAS inhibitors can
413 enhance tumor-specific immunity,[18 19 20] we investigated the activity of ADT-1004 in two
414 PDAC-bearing, syngeneic, immunocompetent mouse models harboring the KRAS^{G12D} mutation.
415 We selected the KRAS^{G12D} mutant luciferase expressing KPC and 2838c3 PDAC lines as both
416 exhibit increased T cell infiltration and an effector phenotype.[15] Moreover, the effector
417 phenotype of CD8^{+} T cells as evidenced by high levels of PD-1 and CTLA4 expression was
418 previously demonstrated in the 2838c3 model is responsive to combinatorial ICB (immune
419 checkpoint blockade) utilizing antagonists to PD-1 and CTLA4.[21] Given our previous findings
420 involving direct injection of ADT-007 in subcutaneous syngeneic mouse PDAC models,
421 including 2838c3,[15] we assessed the numbers and phenotype of T, NK, and myeloid cell subsets
422 by multiplarameter flow cytometry (**Supplementary Figure 2**) to determine whether ADT-1004,
423 as a prodrug of ADT-007, had a similar impact on immune subset abundances and phenotypes in
424 the pancreatic TME.

425 Following 28 days of treatment course (5days/week), mice bearing KPC or 2838c3
426 tumors were euthanized to evaluate changes in the immune cell population densities within the
427 pancreatic TME. ADT-1004 treatment did not alter density (% Total/gm tumor) of innate-like
428 (NKT and γδT) or NK cells in the KPC model (**Supplementary Figure 2A**), compared with the
429 2838c3 model where the densities of innate-like T and NK cell subsets were increased with
430 treatment (**Supplementary Figure 2B**). Furthermore, ADT-1004 treatment increased the density
431 of CD4^{+} and CD8^{+} T cells in the 2838c3 TME (**Figure 3H-I**) despite remaining unchanged in
432 the KPC TME (**Supplementary Figure 3A-B**). Phenotypic analysis revealed that ADT-1004
433 treatment caused a marked increase in the density of CD4^{+} and CD8^{+} PD-1^{+} and CD4^{+} CTLA4^{+}.
434 (**Figure 3H-I**). Furthermore, the densities of CD4^{+} and CD8^{+} T cells co-expressing PD-1,
435 CTLA4, LAG-3, and CD44 (**Figure 3I**) were increased in 2838c3 tumors after ADT-1004
436 treatment, indicating an emergence in exhaustion phenotype. Overall, these findings indicate an
437 increase in the density of activated and potentially exhausted T cells after ADT-1004 treatment.

438 Analysis of myeloid cells after ADT-1004 treatment revealed an increased density (%
439 total/mg tumor) of F4/80^{+} macrophages, XCR1^{+} cDC1, CD172α^{+} cDC2, and Ly6G^{+} granulocytes
440 in the 2838c3, but not KPC TME (**Figure 3J+K and Supplementary Figure 3C**). In each
441 model, F4/80^{+} macrophages exhibited an increase ratio of M1 like (MHCII^{hi}) macrophages
442 compared to M2 (CD206^{+}) like macrophages (**Figure 2F and Figure 3K**). An increase in pro-
443 inflammatory M1 macrophage and dendritic cell subsets is suggestive to a TME allowing for
444 improved anti-tumor immune responses, and increased expression of immune checkpoint
445 receptors PD-1, CTLA4, and LAG-3, indicating a potential benefit of combination with
446 antagonists to these pathway with ADT-1004.

447 **Spatial phenotyping reveals enhancement of TME infiltration in ADT-1004 treated tumors.**

448 We next sought to investigate the effects of ADT-1004 on the cellular infiltration patterns
449 o within the tumor core. Pancreatic tumors from the 2838c3-luc murine PDAC model were
450 initially assessed for viable tumor cores by a licensed veterinary pathologist and 2 mm cores
451 were obtained to generate a microarray of each tumor (n=4 for each treatment group). We
452 performed multiplex immunofluorescence using the Lunaphore COMET system and a 15-plex
453 antibody marker panel for general neoplastic, immune, and stromal cell profiling (**Figure 4A**).
454 Cells were classified into 13 distinct phenotypes based on marker positivity: cancer cells
455 CK^{Bright}, cancer cells CK^{Dim}, B-cells (CD19^{+}), undefined T cells (Tcells (other): CD3^{+}CD8^{-}CD4^{-}
456), cytotoxic T cells (CytoT: CD3^{+} CD8^{+}), T effector cells (Teff: CD3^{+} CD4^{+}), T regulatory cells
457 (Treg: CD3^{+} CD4^{+} Foxp3^{+}), macrophages (Mac: CD11b^{+} Ly6G^{-}), Neutrophils (Neutro: CD11b^{-}
458 Ly6G^{+}), myeloid derived suppressor cells (MDSC: CD11b^{+} Ly6G^{+}), cancer associated
459 fibroblasts (CAF: any combination of FAP^{+}, αSMA^{+}, PDGFRβ^{+}, Desmin^{+}, or Integrinβ3^{+}), and
460 undefined cells (negative for all markers).

461 Initially, count-based metrics showed no significant differences between the treatment
462 groups in the proportion of neoplastic, stromal, or immune cell compartments (**Figure 4A**).
463 Within the neoplastic cellular compartments, there were also no differences in the proportions of
464 cancer cell subtypes, (**Figure 4B**) indicative of epithelial to mesenchymal transformation (EMT)
465 status when assessing mesenchymal marker co-expression (**Figure 4C**). The immune cell counts
466 showed a significant increase in T effector cells in the ADT-1004 treated tumors matching the
467 observations obtained from the dissociative immune phenotyping (**Figure 3H-K, Figure 4D**).
468 Within the stromal compartment there were also no significant differences in the percentages of

469 CAFs both in aggregate and in the single marker expression patterns (**Figure 4E**). There was a
470 trending increase in the number of endothelial and immune cell infiltrate in the ADT-1004
471 treated tumors (**Figure 4F**). These data show minimal differences in the cellular composition of
472 the tumor core microenvironment upon ADT-1004 treatment.

473 To assess effects of ADT-1004 treatment on the cellular infiltration patterns of the core
474 TME, we performed the G-function analysis which quantifies the infiltration of one cell-type
475 (neighbor) within specified radii of another cell type (target). We performed this analysis for sets
476 of 10 µm radii ranging from cell-cell contact distances 10-50 µm through non-cell contact
477 distances (60-200 µm). Significance between vehicle and ADT-1004 were calculated for each
478 pair-wise comparison at each radius. We observed both $Cancer^{CKbright}$ and $Cancer^{CKdim}$ cells had
479 significantly more endothelial cell infiltration in the ADT-1004 treated tumors suggesting better
480 vasculature coverage (**Figure 4G**). In addition to this, we have not identified any significant
481 difference in the proportions of CAF percentage in ADT-1004 treated tumors compared too
482 vehicle (**Figure 4I**). Both $Cancer^{CKdim}$ and CAF cells had increased CytoT cell infiltration within
483 cell-cell contact radii and Teff infiltration within near secretory distances of 100-150µm (**Figure**
484 **4I**, **Supplementary Figure 4A-C**), which correlate with known functions of cell-cell contact and
485 cytokine secretion for these cell types.[22]

486 We next determined if specific mesenchymal markers (αSMA, FAP, Desmin, PDGFRβ,
487 or Integrinβ3) in the target cells were associated with immune cell infiltration patterns.
488 $Cancer^{CKdim}$ cells that co-expressed any mesenchymal marker was not co-localized with the
489 CytoT or Teff cells. This observation confirms previous spatial infiltration observations in mouse
490 and human PDAC samples of reduced T cell infiltration around mesenchymal expressing cancer
491 cells.[23] Analysis of mesenchymal marker expression in the target CAF population showed FAP^+
492 and $Integrin\beta3^+$ CAFs excluded $CD8^+$ T cells in the ADT-1004 treated tumors and $Integrin\beta3^+$
493 CAFs excluded Teff cells; all other mesenchymal markers had no association with immune cell
494 infiltration. Marker expression analysis of the neighbor cells showed that ADT-1004 treated
495 tumors had a significant increase in infiltration of $CD11b^-$ CytoT and Teff cells around
496 $Cancer^{CKdim}$ and CAF cells. These data demonstrate enhancement of immune cell infiltration
497 with ADT-1004 treatment.

498 **ADT-1004 inhibits the growth of KRAS mutant PDX tumors**

499 Given previous reports that ADT-007 inhibits the growth of KRAS mutantcancer cells
500 regardless of the KRAS mutation, we determined the antitumor activity of ADT-1004 across a
501 panel of three PDAC PDX models harboring different KRAS mutations ($KRAS^{G12D}$, $KRAS^{G12C}$,
502 and $KRAS^{G13Q}$) and one pancreaticobiliary PDX model ($KRAS^{G12V}$). Tumor fragments from
503 each of the PDX models were subcutaneously implanted into the right flank of NSG mice. Body
504 weight and tumor volumes were measured while the mice were treated orally with ADT-1004
505 once daily at a dose of 40 mg/kg (5days/week). Tumor weights were determined at the end of the
506 experiment. ADT-1004 treatment significantly inhibited the growth of PDAC tumors with
507 $KRAS^{G12D}$ (**Figure 5A and 5C, Supplemental Figure 5A**), $KRAS^{G12C}$ (**Figure 5E and 5G,**
508 **Supplemental Figure 5B**), $KRAS^{G12V}$ (**Figure 5I and 5K, Supplemental Figure 5C**) and
509 $KRAS^{G13Q}$ (**Figure 5M and 5O, Supplemental Figure 5D**) with no change in body weight over
510 the course of treatment, further demonstrating tolerability at dosages that inhibit tumor growth
511 (**Figure 5B**, **5F**, **5J**, and **5N**, respectively) and therefore the potential for clinical development of
512 ADT-1004 for PDAC.

513 Immunohistochemical (IHC) analysis of four KRAS mutant PDX tumors revealed the
514 multiple effects of ADT-1004 treatment. We have identified a significant reduction of pERK
515 levels in tumors from mice treated with ADT-1004 compared to mice treated with vehicle. In
516 addition, αSMA immunostaining resulted in decreased expression within the ADT-1004
517 treatment group with distinct changes indicating structural reorganization, tissue remodeling, or
518 fibrotic processes. Finally, analysis of Ki-67 levels showed a marked decrease in proliferative
519 activity in all four treatment groups relative to their respective vehicle group, G12D (**Figure 6A**),
520 G12C (**Figure 6B**), G12V (**Figure 6C**) and G13Q (**Figure 6D**) mutant expressing tumors.

521 **ADT-1004 does not inhibit tumor growth of RAS^{WT} PDAC cells**

522 Additional experiments were performed to confirm the RAS selectivity of ADT-1004,
523 given previous studies reporting that RAS^{WT} cancer cells with downstream BRAF mutations
524 were einsensitive to ADT-007.[15] Male NSG mice were implanted subcutaneously with BxPC-3
525 (RAS^{WT} $BRAF^{V600E}$) cells and treated orally with 40 mg/kg ADT-1004 for 31 days. Body weight
526 and tumor volume were monitored twice weekly throughout the study. ADT-1004 treatment did
527 not affect BxPC-3 tumor growth (**Supplementary Figure 6A)** or impacted body weight
528 (**Supplementary Figure 6B**), with no statistically significant difference observed in tumor

529 weights compared to vehicle-treated mice (**Supplementary Figure 6C-6D**). These results lead
530 us to conclude that ADT-1004 inhibits tumor growth as a highly selective pan-RAS inhibitor.

531 **ADT-1004 inhibits tumor growth of PDAC cells resistant to KRAS^{G12C} inhibitors**

532 Human MIA PaCa-2 KRAS^{G12C} cells resistant to KRAS^{G12C} inhibitors (MIA-AMG-Res)
533 were developed as previously described.[16] Resistance to sotorasib and adagrasib was intitally
534 confirmed by *in vitro* experiments to determine growth IC_{50} values against the parental MIA
535 PaCa-2 cells. MIA PaCa-2 cells showed remarkable sensitivity to ADT-007 with an IC_{50} value
536 of 3 nM, while sotorasib and adagrasib were less potent with IC_{50} values of 28 and 21 nM,
537 respectively, and caused less overall growth inhibition (**Figure 7A)**. MIA-AMG-Res cells were
538 only slightly less sensitive to ADT-007 with an IC_{50} value of 16 nM, but completely lost
539 sensitivity to sotorasib and adagrasib **(Figure 7B**). In addition, ADT-007, sotorasib, and
540 adagrasib inhibited colony formation in parental MIA PaCa2 cells. However, the differences in
541 potency and extent of killing caused by ADT-007 compared with sotorasib and adagrasib were
542 more pronounced, which may reflect the ability of ADT-007 to induce mitotic arrest and
543 apoptosis as previously reported.[15] Similar to growth assays, ADT-007 retained activity to inhibit
544 colony formation in MIA-AMG-Res cells, while sensitivity to sotorasib and adagrasib was
545 markedly diminished (**Figure 7C** and **7D**).

546 Next, experiments utilizing NSG mice xenografted subcutaneously with parental MIA
547 PaCa-2 and MIA-AMG-Res cells were conducted. Parental MIA PaCa-2 cells showed
548 comparable decreased tumor volume (**Figure 7E**) and final tumor weights (**Figure 7F** and **7G**),
549 following treatment with ADT-1004, sotorasib or adagrasib in which each were tested at a once-
550 daily dose of 40 mg/kg (5days/week). No significant differences in body weight were measured
551 across treatment and vehicle groups (**Supplementary Figure 7A**). In addition, we found a
552 significant reduction in pERK levels in tumor tissues in all the treatment groups compared to
553 vehicle-treated mice tumor tissues (**Figure 7H** and **Supplementary Figure 7C)**. In a side-by-
554 side comparision, oral administration of ADT-1004 led to a dramatic decrease in tumor volume
555 (**Figure 7I**) and weight (**Figure 7J** and **7K**) compared with vehicle against tumors derived from
556 MIA-AMG-Res cells. By contrast, neither sotorasib nor adagrasib were effective. Notably,
557 ADT-1004 demonstrated antitumor activity without any visible change in the body weights of
558 treated mice (**Supplementary Figure 7B**). Furthermore, western blotting for the detection of
559 pERK showed a significant reduction in the ADT-1004 treated tumors compared to all other

560 treatment or vehicle groups, while meither sotorasib or adagrasib impacted pERK levels (**Figure**
561 **7L** and **Supplementary Figure 7D)**. These results show that ADT-1004 is highly effective
562 against $KRAS^{G12C}$ tumors resistant to sotorasib or adagrasib, suggesting the potential to treat
563 patiesnts who fail therapy with $KRAS^{G12C}$ inhibitors.
564

565 **Discussion**

566 PDAC poses a formidable global health challenge as the most lethal cancer with a notable
567 absence of effective treatments.[24] Point mutations in the RAS oncogene family, encompassing
568 KRAS, NRAS, and HRAS are widespread across multiple cancers, but especially mutations in
569 KRAS as a driver of PDAC. Despite the high prevalence of KRAS mutations in the most fatal
570 human cancers, direct targeting of KRAS by reversible inhibitors has been challenging primarily
571 because of the lack of binding surfaces on the protein and high affinity to bind GTP to inhibit
572 GTP activation of effector interactions. The recent FDA approval of covalent $KRAS^{G12C}$
573 inhibitors for the treatment of non-small cell lung cancer has renewed optimism to study RAS as
574 a druggable target, although currently available $KRAS^{G12C}$ inhibitors have limited use for PDAC
575 given that $KRAS^{G12C}$ mutations are rare in patients diagnosed with PDAC. Recognizing the role
576 of other KRAS mutations in PDAC and other cancers, namely $KRAS^{G12D}$, intensive efforts are
577 ongoing to develop $KRAS^{G12D}$ inhibitors.[25] However, given that adaptive resistance is a crucial
578 limitation of $KRAS^{G12C}$ inhibitors that is attributed to various compensatory mechanisms, for
579 example, from new KRAS mutations or activation of RAS^{WT} isoforms, likely other allele-
580 specific inhibitors will have similar limitations.[14]

581 This present study builds upon our discovery of ADT-007, a reversible, highly potent,
582 and selective pan-RAS inhibitor, with broad growth inhibitory activity and potential to avoid
583 resistance mechanisms limiting the efficacy of mutant or isoform specific RAS inhibitors.[15] As
584 ADT-007 has low water solubility and is rapidly metabolized by glucuronidation, which limits
585 systemic exposure by systemic IV or oral administration, we developed ADT-1004 as an orally
586 bioavailable prodrug of ADT-007. Oral administration of ADT-1004 in mice generated sustained
587 plasma levels of ADT-007 that was amenable to once or twice-daily dosing schedules, which
588 produced appreciably higher ADT-007 concentrations than required to inhibit PDAC cell growth
589 *in vitro*. The difference between the maximum tolerated dose of 175 mg/kg ADT-1004 twice-

590 daily and the minimally effective dose of 40 mg/kg once-daily is relatively large, suggesting that
591 ADT-1004 will have a broad therapeutic window in the clinic.

592 Here we showed antitumor activity of orally administered ADT-1004 against multiple
593 mouse models of PDAC, including orthotopically implanted mouse cell lines and subcutaneously
594 implanted PDX with different KRAS mutations. In these models, we consistently observed
595 antitumor activity of ADT-1004 at a once-daily dose of 40mg/kg. Although higher dosages or a
596 more frequent dosing schedule may result in greater antitumor activity, we selected 40 mg/kg as
597 a minimal dosage that appeared to generate maximum plasma levels of ADT-007. In addition,
598 this dosage demonstrated strong inhibitory effects on RAS activation and downstream signaling
599 by measurement of RAS-GTP and pERK levels, respectively. These findings are also consistent
600 with the published activity of other mutation specific and pan-Ras inhibitors in PDAC. [26, 27, 28, 29],
601 although further studies are needed to determine which mechanism of inhibiting RAS will result
602 in greater efficacy, tolerability, and the greatest potential to avert resistance.

603 A major challenge in using immune therapy for the treatment of PDAC has been the level
604 of dysregulation of the immune system at multiple levels, including low T cells, exhausted T
605 cells, absent antigen presenting cells and high inhibitory tumor-associated macrophages.
606 Oncogenic KRAS is a significant enabler of the immune suppressive TME in PDAC such that
607 blockage of RAS signaling promotes cytotoxic and M1 pro-inflammatory anti-tumor immune
608 responses.[30] Preclinical studies of mutant specific KRAS inhibitors, demonstrates a critical role
609 of oncogenic KRAS signaling in immune suppression whereby targeting RAS vastly improves
610 tumor immune responses.[31] Our study demonstrates similar immune modulatory potential of
611 ADT-1004 in comparison with other mutation-specific and pan-RAS inhibitors.[18, 20, 29, 32]
612 Specifically, treatment with ADT-1004 increases immune infiltration into the TME with
613 increases in T cells infiltrations. Furthermore, there is an increase in T cells expressing immune
614 suppressive receptors PD-1, CTLA4, and LAG-3, which are critical for immunosuppression of
615 anti-tumor specific T cell responses.[33, 34] Others have demonstrated that targeted inhibition of
616 oncogenic $KRAS^{G12D}$ signaling with MRTX1133 in pre-clinical models of PDAC resulted in
617 increases in PD-1, such that blockade of this signaling pathway enhanced antitumor efficacy.[18,32]
618 Therefore, it is likely that ADT-1004 could enhance efficacy in comibination with agonists to
619 PD-1 and CTLA4, although further studies are needed to assess this possibility along with
620 tolerability. The observed increase in macrophage populations indicate a role for ADT-1004 in

621 alteration of the macrophage phenotype from an immunosuppressive anti-inflammatory (M2
622 like) to a pro-inflammatory (M1 like) phenotype, which is again consistent with findings using
623 targeted inhibitors. Additionally, we observed increases in the abundance of dendritic cell
624 subsets, which are critical for priming tumor-antigen specific T cells.[35] Interestingly $CD11b^+$
625 $Ly6G^+$ granulocytes in the 2838c3 TME were increased with ADT-1004 treatement. These cells
626 expressed a significant, but modest increase in MHCII and downregulation of PD-L1, suggesting
627 that these cells may exhibit antigen-presentation potential, which has been associated with
628 increased survival in patients with a range of cancers and highlight another novel property of
629 ADT-1004 to impact.[36] Overall, this broad activation of macrophages (and granulocytes) with
630 enhanced T cell priming capabilities suggests the potential of ADT-1004 to enhance antigen
631 presentation and pro-inflammatory responses in the pancreatic TME.

632 Our spatial analysis of tumor core regions shows cell localization patterns were enhanced
633 by ADT-1004 treatment. Of interest, is the enhancement of spatial patterns known in cancer
634 biology as the paucity of infiltration of immune cells around mesenchymal-transitioned cancer
635 cells and FAP^+ and $Integrin\beta3^+$ CAFs. Combined with the observations of cancer cell line
636 specific differences in immunological phenotypes, these observations suggest that tumor growth
637 suppression by ADT-1004 treatment impacts host response mechanisms that are cancer specific.
638 This activity also opens the possibilities for future combination therapies with TME targeting
639 approaches.

640 Another desirable feature of ADT-1004 is its cytotoxic ability towards PDAC cells
641 resistant to FDA-approved mutant-specific KRAS inhibitors. In this study, we show that human
642 MIA PaCa-2 PDAC cells harboring $KRAS^{G12C}$ developed to be resistant to sotorasib and
643 adagrasib retained sensitivity to ADT-007 *in vitro* and to ADT-1004 *in vivo*. By contrast, both
644 sotorasib and adagrasib essentially lost activity *in vitro* as determined by growth and colony
645 formation assays and *in vivo* using a subcutaneous mouse tumor model. Previous clinical studies
646 with $KRAS^{G12C}$ inhibitors have identified multiple mechanisms of intrinsic or acquired
647 resistance. These include new mutations in KRAS or activation of the wild-type KRAS allele or
648 compensation from RAS WT isozymes (e.g., NRAS or HRAS) that are co-expressed with mutant
649 KRAS and activated by growth factors (e.g., EGF) enriched in the TME.[14] These resistance
650 mechanisms can be bypassed by a pan-RAS inhibitor such as ADT-1004 and provide a key
651 advantage over existing mutant-specific KRAS inhibitors to support clinical development. The

652 ability of ADT-007 to induce mitotic arrest and apoptosis may provide additional advantages to
653 avert resistance as previously reported.[15] For example, ADT-007 completely inhibited colony
654 formation of $KRAS^{G12C}$ PDAC cells, while $KRAS^{G12C}$ inhibitors (sotorasib and adagrasib),
655 KRAS-specific inhibitors (BI-2865) and another pan-RAS inhibitor in development (RMC-6236)
656 were appreciably less effective.

657 This comprehensive study establishes ADT-1004 as a 1st-in-class orally bioavailable pan-
658 RAS inhibitor with promising antitumor efficacy against KRAS-mutant PDAC, including
659 resistant phenotypes, which could be considered as a monotherapy. The changes in the TME
660 observed with ADT-1004 also suggest that a combination with immune checkpoint inhibitors is a
661 rational approach to evaluate in preclinical models.
662

663 **References**

664 1. Yousef A, Yousef M, Chowdhury S, et al. Impact of KRAS mutations and co-mutations on clinical
665 outcomes in pancreatic ductal adenocarcinoma. NPJ Precision Oncology 2024;8:27.
666 2. Mizrahi JD, Surana R, Valle JW, et al. Pancreatic cancer. The Lancet 2020;395:2008-2020.
667 3. Siegel RL, Miller KD, Wagle NS, et al. Cancer statistics, 2023. CA: a cancer journal for clinicians
668 2023;73.
669 4. Jiang Y, Sohal DP. Pancreatic adenocarcinoma management. JCO Oncology Practice 2023;19:19-
670 32.
671 5. Siegel RL, Giaquinto AN, Jemal A. Cancer statistics, 2024. CA: a cancer journal for clinicians
672 2024;74.
673 6. Bailey P, Chang DK, Nones K, et al. Genomic analyses identify molecular subtypes of pancreatic
674 cancer. Nature 2016;531:47-52.
675 7. Lee JK, Sivakumar S, Schrock AB, et al. Comprehensive pan-cancer genomic landscape of KRAS
676 altered cancers and real-world outcomes in solid tumors. NPJ Precision Oncology 2022;6:91.
677 8. McCormick F. KRAS as a therapeutic target. Clinical Cancer Research 2015;21:1797-1801.
678 9. Ryan DP, Hong TS, Bardeesy N. Pancreatic adenocarcinoma. New England Journal of Medicine
679 2014;371:1039-1049.
680 10. Waters AM, Der CJ. KRAS: the critical driver and therapeutic target for pancreatic cancer. Cold
681 Spring Harbor perspectives in medicine 2018;8:a031435.
682 11. Ostrem JM, Peters U, Sos ML, et al. K-Ras (G12C) inhibitors allosterically control GTP affinity and
683 effector interactions. Nature 2013;503:548-551.
684 12. Lanman BA, Allen JR, Allen JG, et al. Discovery of a Covalent Inhibitor of KRASG12C (AMG 510)
685 for the Treatment of Solid Tumors: ACS Publications, 2019.
686 13. Liu JO. Targeting cancer with molecular glues. Science 2023;381:729-730.
687 14. Awad MM, Liu S, Rybkin II, et al. Acquired resistance to KRASG12C inhibition in cancer. New
688 England Journal of Medicine 2021;384:2382-2393.
689 15. Foote JB, Mattox TE, Keeton AB, et al. A Novel Pan-RAS Inhibitor with a Unique Mechanism of
690 Action Blocks Tumor Growth in Mouse Models of GI Cancer. bioRxiv 2024.
691 16. Khan HY, Nagasaka M, Aboukameel A, et al. Anticancer efficacy of KRASG12C inhibitors is
692 potentiated by PAK4 inhibitor KPT9274 in preclinical models of KRASG12C mutant pancreatic
693 and lung cancers. bioRxiv 2023:2023.03. 27.534309.
694 17. Garcia PL, Council LN, Christein JD, et al. Development and histopathological characterization of
695 tumorgraft models of pancreatic ductal adenocarcinoma. PloS one 2013;8:e78183.
696 18. Canon J, Rex K, Saiki AY, et al. The clinical KRAS (G12C) inhibitor AMG 510 drives anti-tumour
697 immunity. Nature 2019;575:217-223.
698 19. Mugarza E, van Maldegem F, Boumelha J, et al. Therapeutic KRASG12C inhibition drives effective
699 interferon-mediated antitumor immunity in immunogenic lung cancers. Science advances
700 2022;8:eabm8780.
701 20. Kemp SB, Cheng N, Markosyan N, et al. Efficacy of a small-molecule inhibitor of KrasG12D in
702 immunocompetent models of pancreatic cancer. Cancer discovery 2023;13:298-311.
703 21. Li J, Byrne KT, Yan F, et al. Tumor cell-intrinsic factors underlie heterogeneity of immune cell
704 infiltration and response to immunotherapy. Immunity 2018;49:178-193. e7.
705 22. Thurley K, Gerecht D, Friedmann E, et al. Three-dimensional gradients of cytokine signaling
706 between T cells. PLoS computational biology 2015;11:e1004206.
707 23. Carstens JL, Yang S, De Sampaio PC, et al. Stabilized epithelial phenotype of cancer cells in
708 primary tumors leads to increased colonization of liver metastasis in pancreatic cancer. Cell
709 reports 2021;35.

710 24. Neoptolemos JP, Kleeff J, Michl P, et al. Therapeutic developments in pancreatic cancer: current
711 and future perspectives. Nature reviews Gastroenterology & hepatology 2018;15:333-348.
712 25. Tang D, Kang R. Glimmers of hope for targeting oncogenic KRAS-G12D. Cancer Gene Therapy
713 2023;30:391-393.
714 26. Hallin J, Bowcut V, Calinisan A, et al. Anti-tumor efficacy of a potent and selective non-covalent
715 KRASG12D inhibitor. Nature medicine 2022;28:2171-2182.
716 27. Wasko UN, Jiang J, Dalton TC, et al. Tumor-selective activity of RAS-GTP inhibition in pancreatic
717 cancer. Nature 2024:1-3.
718 28. Holderfield M, Lee BJ, Jiang J, et al. Concurrent inhibition of oncogenic and wild-type RAS-GTP
719 for cancer therapy. Nature 2024:1-8.
720 29. Jiang J, Jiang L, Maldonato BJ, et al. Translational and therapeutic evaluation of RAS-GTP
721 inhibition by RMC-6236 in RAS-driven cancers. Cancer Discovery 2024;14:994-1017.
722 30. Ischenko I, D'Amico S, Rao M, et al. KRAS drives immune evasion in a genetic model of
723 pancreatic cancer. Nature communications 2021;12:1482.
724 31. Molina-Arcas M, Downward J. Exploiting the therapeutic implications of KRAS inhibition on
725 tumor immunity. Cancer Cell 2024;42:338-357.
726 32. Mahadevan KK, McAndrews KM, LeBleu VS, et al. KRASG12D inhibition reprograms the
727 microenvironment of early and advanced pancreatic cancer to promote FAS-mediated killing by
728 CD8+ T cells. Cancer Cell 2023;41:1606-1620. e8.
729 33. He X, Xu C. Immune checkpoint signaling and cancer immunotherapy. Cell research
730 2020;30:660-669.
731 34. Sharpe AH, Pauken KE. The diverse functions of the PD1 inhibitory pathway. Nature Reviews
732 Immunology 2018;18:153-167.
733 35. Gardner A, de Mingo Pulido Á, Ruffell B. Dendritic cells and their role in immunotherapy.
734 Frontiers in immunology 2020;11:924.
735 36. Wu Y, Ma J, Yang X, et al. Neutrophil profiling illuminates anti-tumor antigen-presenting
736 potency. Cell 2024;187:1422-1439. e24.

737

738 **Figure Legends:**

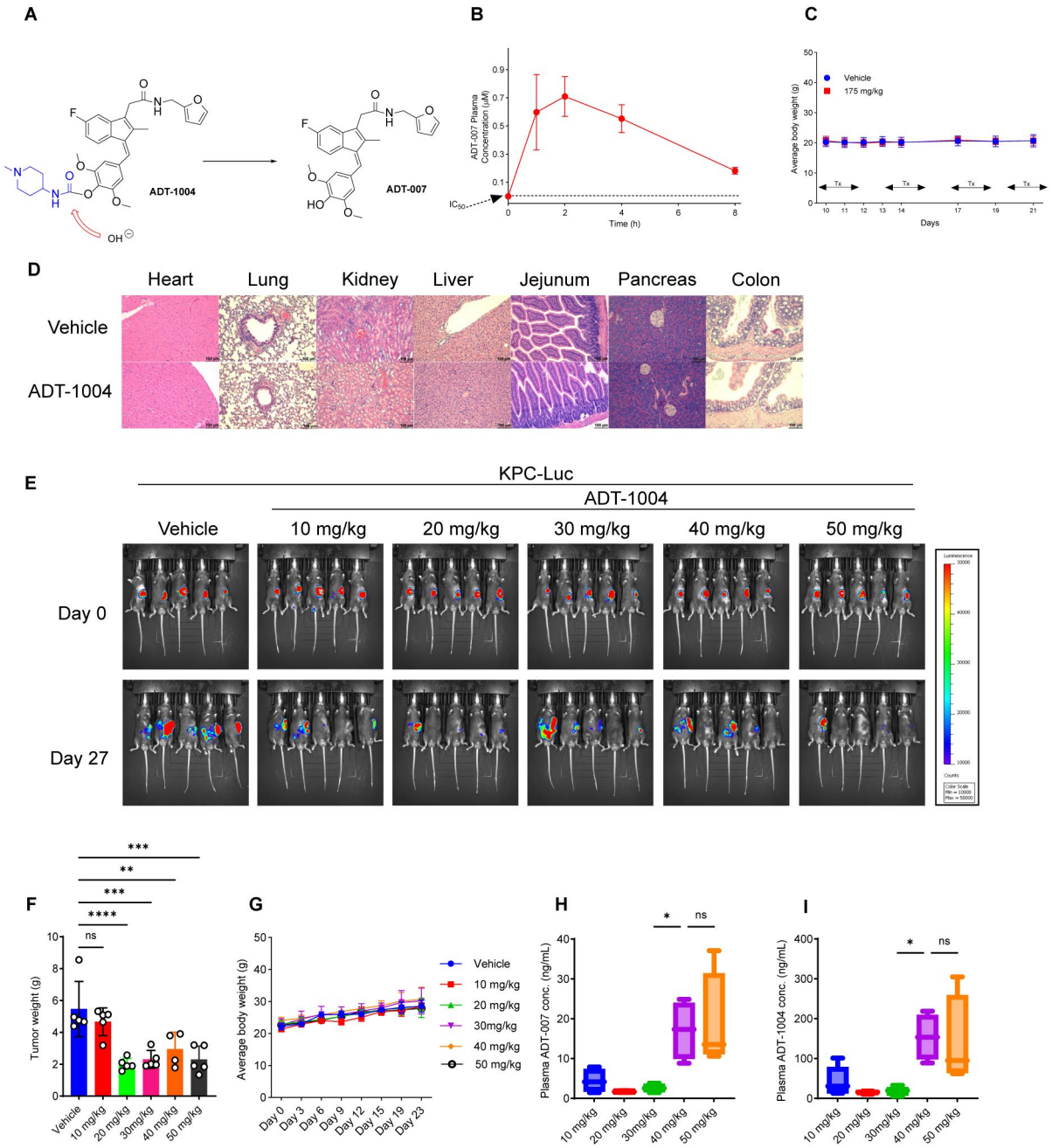

Figure 1: Evaluation of ADT-1004 efficacy and toxicity profile in murine model of pancreatic cancer.

(**A**)**.** Chemical structures of ADT-1004 and ADT-007. **(B).** Plasma levels of ADT-007 in mice following a single oral administration of ADT-1004 (100 mg/kg, mean ± SD, n=3-4). **(C).** Body weights of C57BL/6 mice treated with ADT-1004 (175 mg/kg, n=5) or vehicle (n=10) orally BID, 5days/week for 3.5 weeks (mean ± SD). (**D**). Histopathological examination of vital organs (heart, lung, kidney, liver, jejunum, pancreas, and colon) from mice treated with ADT-1004 at

747 175 mg/kg BID as assessed by H&E staining. (**E**). *F*-Luc-labeled KPC cells were orthotopically
748 implanted into C57BL/6J mice (n=30). After 1 week, group of 5 mice were orally administered
749 vehicle or ADT-1004 (10, 20, 30, 40, and 50 mg/kg). Bioluminescence images at the indicated
750 time points are shown. (**F**). Tumors were weighed at the end of the experiment under the
751 indicated conditions for experiment in (**E**). (**G**). Average body weights of the animals during the
752 course of the treatment shown in experiment (**E**). (**H**). The concentration of ADT-007 in plasma
753 of mice on the last day of treatment is depicted as mean alongside SD. (**I**). The concentration of
754 ADT-1004 in plasma of mice on the last day of treatment is depicted as geometric mean
755 alongside standard deviation. ADT-007 and ADT-1004 levels measured by LC-MS/MS. All
756 quantitative data represent the mean ± SEM. ns, non-significant, $*p < 0.05$, $**p < 0.01$, $***p <$
757 0.001, and $****p < 0.0001$.

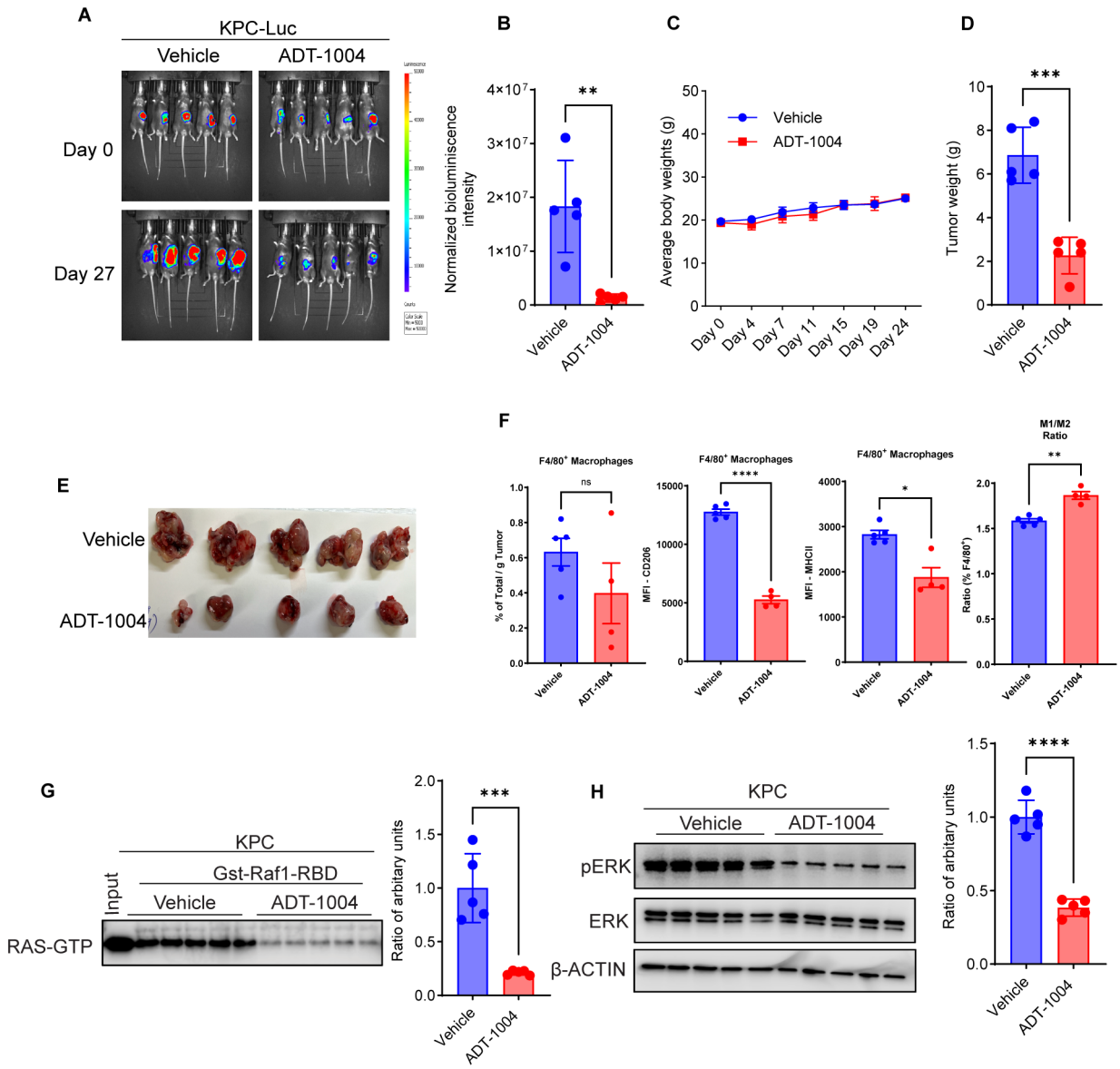

Figure 2: Effect of ADT-1004 treatment on tumor growth and molecular markers in KPC cell-implanted C57BL/6J mice.

(A). KPC-Luc cells were injected orthotopically into the pancreas of C57BL/6J mice. Mice were treated by oral gavage 5days/week with vehicle or 40 mg/kg ADT-1004 and sacrificed after 27 days of treatment. Representative bioluminescence images at the indicated time points are shown. **(B).** Relative normalized whole-body bioluminescence intensities in mice under the indicated conditions (n=5). **(C).** Average body weights of mice treated with vehicle and ADT-1004 (40 mg/kg). **(D).** Tumor weights were measured from mice at the end of the experiment under the indicated conditions for experiment in (**A**). **(E).** Tumor images at the end of the experiment are shown. (**F**) The percentages of $CD45^+$ $CD11b^+$ F4/80, and $CD206^+$

769 (macrophages), $CD11b^+$ $F4/80^+$ $PD\text{-}L1^+$, and M1/M2 ratios increased in tumors from ADT-1004
770 treated (n=4) compared to vehicle (n=5) treated mice. Welch's t-test determined p values. Error
771 bars indicate SD. **(G).** Ithe tumors were probed for detecting activated RAS GTP levels by GST-
772 Raf1-RBD pull-down assay (left) and graph depicting quantifyication of activated RAS GTP
773 levels (right). **(H).** Indicated tumor tissues were analyzed for pERK and total ERK by
774 immunoblotting. β-Actin was used as a loading control (left). Graph depicting quantifyication of
775 pERK by western blot analysis, normalized using β-Actin (right). All quantitative data represent
776 the mean ± SEM. ns, non-significant, $*p < 0.05$, $**p < 0.01$, $***p < 0.001$, and $****p < 0.0001$.
777

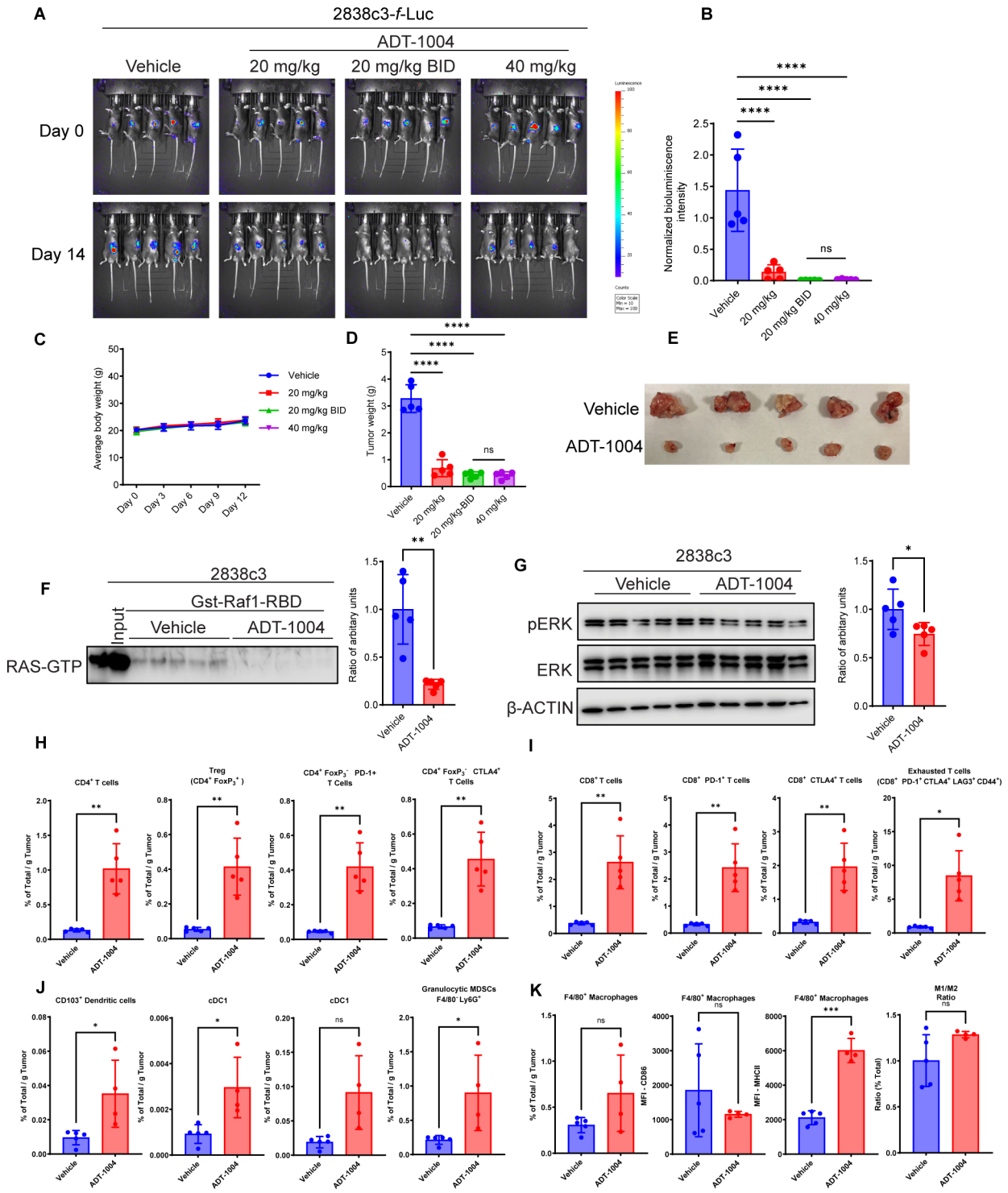

Figure 3: ADT-1004 treatment suppresses tumor growth and modulates tumor microenvironment in C57BL/6J mice with 2838c3 cell implants.

(A). F-Luc-labeled 2838c3 cells were orthotopically implanted into C57BL6/J mice (n=20). Four groups of 5 mice were treated with vehicle or ADT-1004 by oral gavage (20 mg/kg, 20 mg/kg

783 BID, and 40 mg/kg body weight) 5 days/week per week. **(B).** Normalized bioluminescence
784 intensities of the tumors in the 4 groups of mice at day 14 are shown. **(C).** Average body
785 weights of the animals during the course of the treatment shown in experiment (**A**). **(D)**. Tumor
786 weights were measured from mice at the end of the experiment for indicated dosing schedules
787 (**A**). (**E**). Tumor images at the end of the experiment are shown for vehicle and ADT-1004 (40
788 mg/kg). (**F**). Indicated tumor tissues were probed for detecting activated RAS GTP levels by
789 GST-Raf1-RBD pull-down assay (left). Graph depicting the quantification of activated RAS
790 GTP levels (right). (**G**). Indicated tumor tissues were analyzed for pERK and total ERK. β-Actin
791 was used as a loading control (left). Graph depicting the quantification of pERK in western blot
792 analysis, normalized using β-Actin (right). (**H**). Proportions of $CD4^+$ T-cells, $CD4^+$ $Foxp3^+$,
793 $CD4^+$ PD-1^+ T cells, and $CD4^+$ CTLA-4^+ T cells in 2838c3 TiME were determined by multi-
794 parameter flow cytometry in ADT-1004 (n=5) and vehicle (n=5) treated mice. Welch's unpaired
795 t-test determined p values, ns indicates not significant. Error bars indicate SD. (**I**). Expression of
796 $CD8^+$ T-cells, $CD8^+$ PD-1^+ T cells, $CD8^+$ PD-1^+ $LAG3^+$, and $CD8^+$ PD-1^+ CTLA-4^+ subsets from
797 2838c3 TME. Welch's t-test determined p values and error bars indicate SD. (**J**). The percentages
798 of $CD11b^+$ $MHCII^{hi}$, $XCR1^+$ cDC1, and $CD11b^+$ $CD11c^{hi}$ MHCII ^{hi} $CD172\alpha^+$ cDC2 subsets
799 increased in ADT-1004 (n=5) compared to vehicle (n=5) treated mice. Welch's t-test determined
800 p values; ns indicates not significant. Error bars indicate SD. (**K**). The percentages of $CD45^+$
801 $CD11b^+$ F4/80, and $CD206^+$ (macrophages), $CD11b^+$ $F4/80^+$ PD-$L1^+$, M1/M2 ratio increased in
802 ADT-1004 treated (n=5) compared to vehicle (n=5) treated mice. Welch's t-test determined p
803 values. Error bars indicate SD. ns, non-significant, $*p < 0.05$, $**p < 0.01$, $***p < 0.001$, and
804 $****p < 0.0001$.
805
806
807
808
809
810

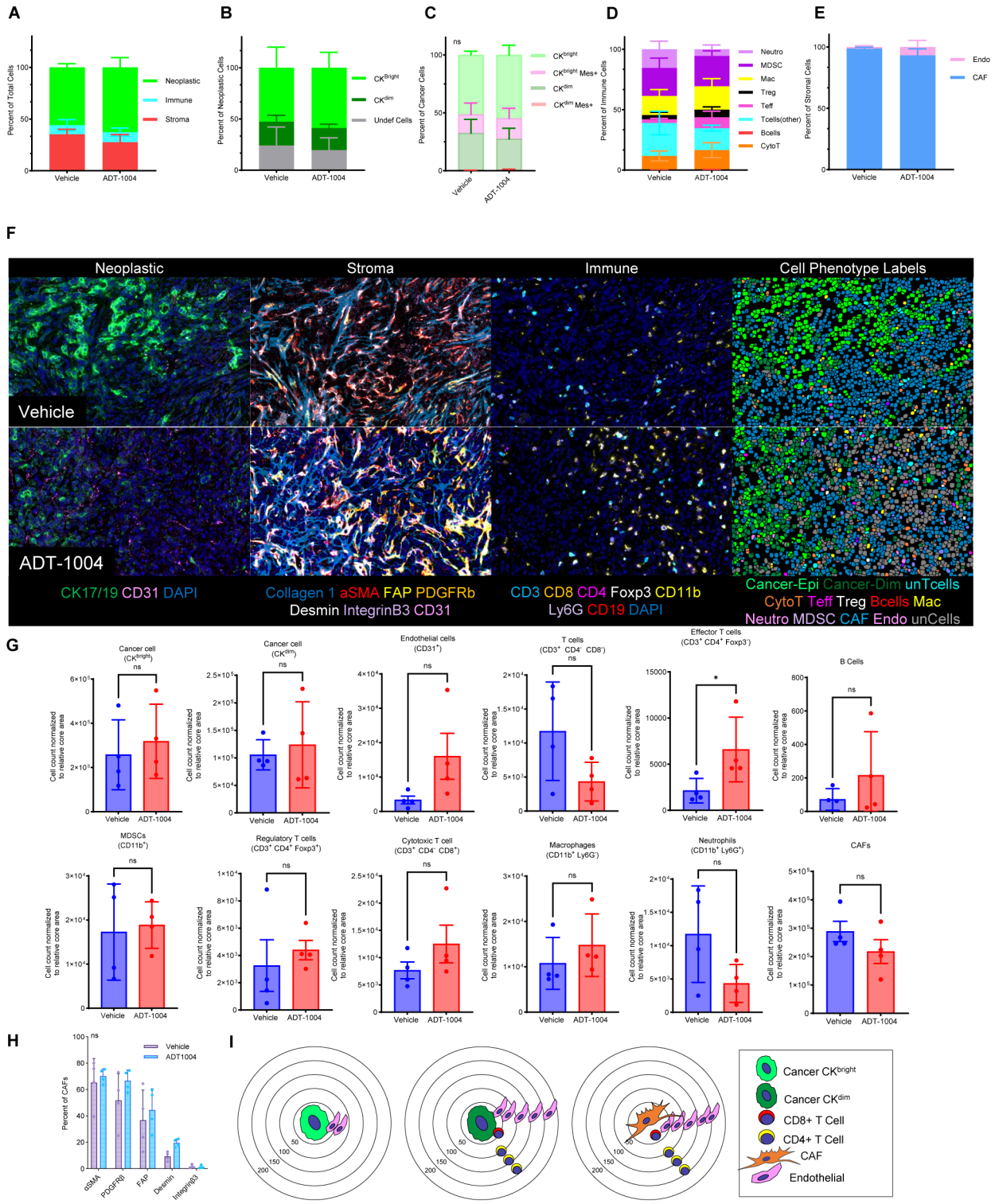

Figure 4: Spatial quantification reveals increased immune infiltration in ADT-1004 treated TME.

(A). The expression matrix for each of the cell phenotypes based on Visiopharm results. **(B).** Percentage of neoplastic cells (y-axis) in each tumor (color legend) for each core of the TMA (x-

axis). **(C).** Mesenchymal expressing CK^{dim} cells in ADT-1004 treated tumors did not co-localize with CD8+ or CD4+ T cells. **(D).** Percentage of immune cells (y-axis) in each tumor (color legend) for each core of the TMA (x-axis). **(E).** Annotations of classified neoplastic and immune cells (top) in the vehicle (left) and ADT-1004 treatments (right) and the corresponding antigens detected in the multi-color fluorescence images (bottom). **(F).** The t-distributed stochastic neighbor embedding (tSNE) plot showed 13 clusters (color legend) in a single core (left). Expression programs of different cell phenotypes (right) in the vehicle and ADT-1004 treated cores. tSNEs of single-nucleus profiles (dots) of neoplastic cells (cancer-epi, cancer-dim, and CAFs) from all tumors, and immune compartments (Macrophages, cyto T cells, T cells, Teff, and Tregs). **(G).** Unchanged CK^{bright} and CK^{dim} cells and increasing trend in endothelial cell infiltration in ADT-1004 treated TMAs compared to vehicle. Unchanged Tregs, significantly increased Teff, increased Teff/Treg ratio, and increased B cells in ADT-1004 treated TMAs compared to vehicle. Increased monocytic MDSCs ($CD11b^+$ $Ly6G^-$) and decreased granulocytic MDSCs ($CD11b^+$ $Ly6G^+$) in ADT-1004 treated TMAs compared to vehicle. Slightly reduced CAFs and increased endothelial cells in ADT-1004 treated TMAs compared to vehicle. **(H).** Unchanged percentage of CAFS in (α-SMA, PDGFRβ, FAP, Desmin, and Integrinβ3). **(I).** Reduced pericytic coverage in ADT-1004 treated tumors compared to vehicle in endothelial cells (left). Mesenchymal expressing CK^{dim} cells in ADT-1004 treated tumors did not co-localize with $CD8^+$ or $CD4^+$ T cells (middle). FAP^+ and Integrinβ3^+ CAFs exclude $CD8^+$ T cells Integrinβ3^+ CAFs exclude $CD4^+$ T cells (right). ns: not significant and $*p < 0.05$.

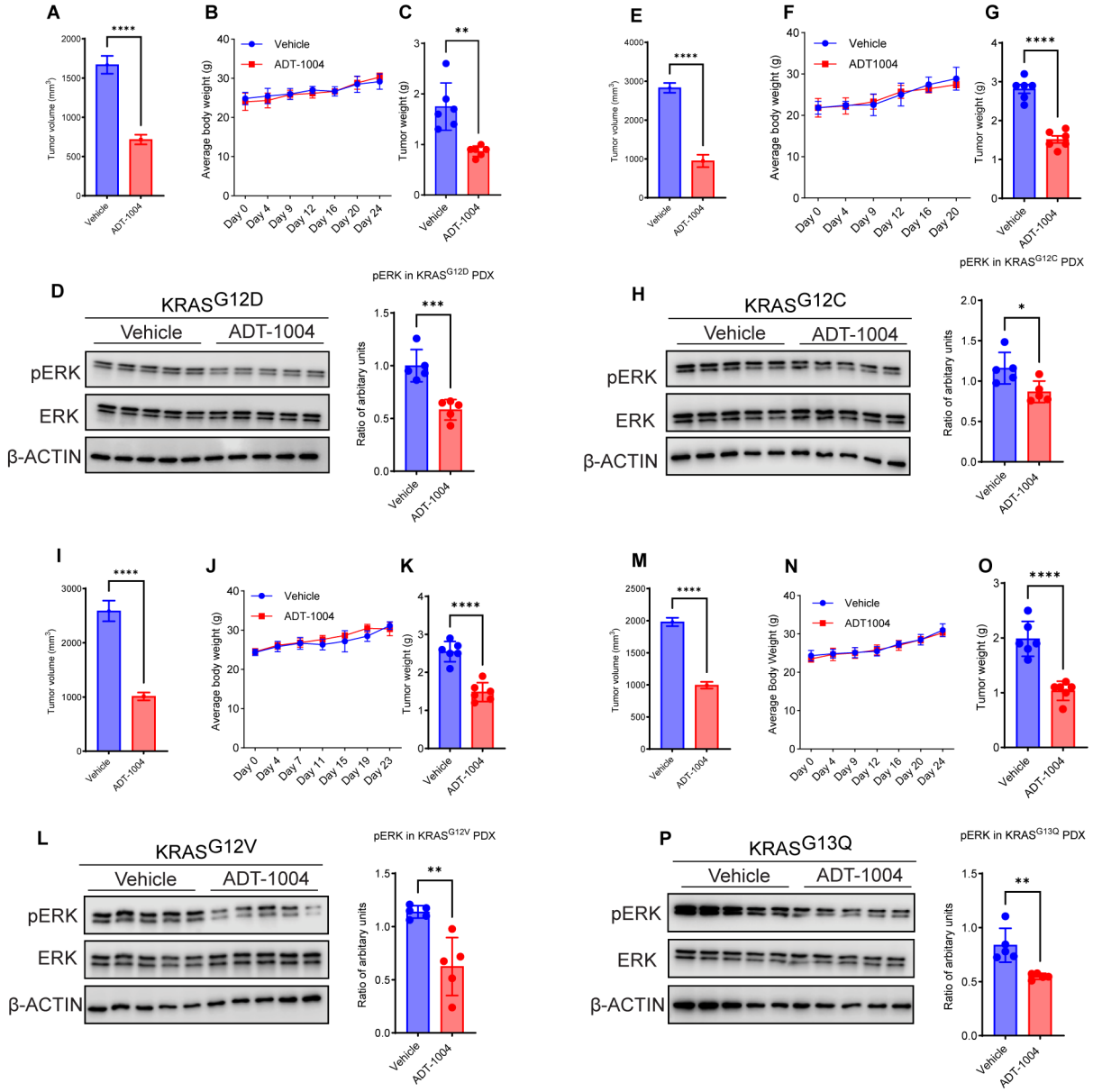

Figure 5: ADT-1004 treatment suppresses tumor growth and downregulates pERK levels in KRAS-mutant PDX models.

(**A-D**). KRAS^{G12D} PDX. (**A**) Tumor growth curves of KRAS^{G12D} PDX implanted subcutaneously into NSG mice and treated with vehicle or ADT-1004 (n=6). (**B**). Average body weights of mice treated with vehicle and ADT-1004 (40 mg/kg). (**C**). Tumor weights were measured from mice at the end of the experiment under the indicated conditions for experiment in (**A**). (**D**). The indicated tumor tissues were probed for measuring pERK and total ERK. β-Actin was used as a loading control. Graph depicting the quantification of pERK by western blot analysis, normalized using β-Actin (left). (**E-H**) KRAS^{G12C} PDX. (**E**) Tumor growth curves of KRAS^{G12C}

850 PDX implanted subcutaneously into NSG mice (n=6). (**F**). Body weights of mice treated with
851 vehicle and ADT-1004 (40 mg/kg). (**G**). Tumor weights were measured from mice at the end of
852 the experiment under the indicated conditions for experiment in (**E**). (**H**). The indicated tumor
853 tissues were probed for measuring pERK and total ERK. β-Actin was used as loading control
854 (right). Graph depicting the quantification of pERK by western blot analysis, normalized using
855 β-Actin (left). (**I-L**). $KRAS^{G12C}$ PDX. (**I**). Tumor growth curves of $KRAS^{G12V}$ PDX implanted
856 subcutaneously into NSG mice (n=6). (**J**). Average body weights of the animals during the
857 course of the treatment shown in the experiment. (**K**). Tumor weights were measured from mice
858 at the end of the experiment under the indicated conditions for experiment in (**I**). (**L**). The
859 indicated tumor tissues were probed for measuring pERK and total ERK. β-Actin was used as
860 loading control (right). Graph depicting the quantification of pERK by western blot analysis,
861 normalized using β-Actin (left). (**M-P**) $KRAS^{G13Q}$ PDX. (**M**)Tumor growth curves of $KRAS^{G13Q}$
862 PDX implanted subcutaneously into NSG mice (n=6). (**N**). The average body weights of the
863 animals during the treatment are shown in the experiment. (**O**) Tumor weights were measured
864 from mice at the end of the experiment under the indicated conditions for experiment in (**M**). (**P**)
865 The indicated tumor tissues were probed for measuring pERK and total ERK. β-Actin was used
866 as loading control (right). Graph depicting the quantification of pERK by western blot analysis,
867 normalized using β-Actin (left). Data represent the mean ± SEM. *$p < 0.05$, **$p < 0.01$, ***$p <$
868 0.001, and ****$p < 0.0001$.
869
870
871
872
873
874

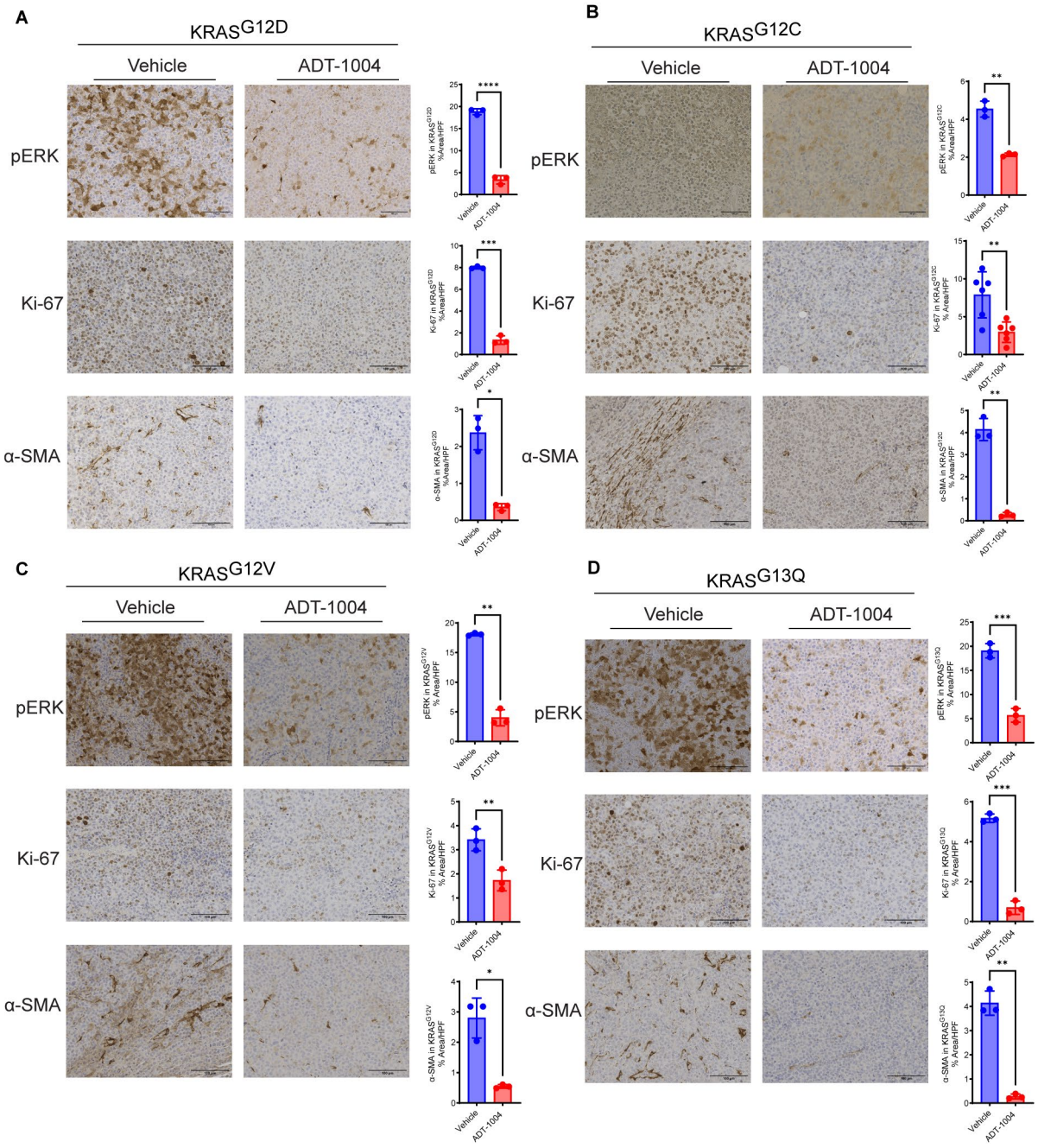

875

876 **Figure 6: ADT-1004 treatment downregulates molecular markers in KRAS-mutant PDX**
877 **models.**

878 (**A**) Representative IHC images of pERK, αSMA, and Ki-67 (left) and quantifications of IHC
879 results (right) in $KRAS^{G12D}$ PDX model. (**B**). Representative IHC images of pERK, αSMA, and
880 Ki-67 (left) and quantifications of IHC results (right) in $KRAS^{G12C}$ PDX model. (**C**).
881 Representative IHC images of pERK, αSMA, and Ki-67 (left) and quantifications of IHC results
882 (right) in $KRAS^{G12V}$ PDX model. (**D**). Representative IHC images of pERK, αSMA, and Ki-67

883 (left) and quantifications of IHC results (right) in $KRAS^{G13Q}$ PDX model. Results reveal that
884 these proteins are highly expressed in KRAS mutations (G12D, G12V, G12C, and G13Q) and
885 reduced expression in ADT-1004 treated tumors. Data represent the mean ± SEM. *$p < 0.05$,
886 **$p < 0.01$, ***$p < 0.001$, and ****$p < 0.0001$.
887
888
889
890
891

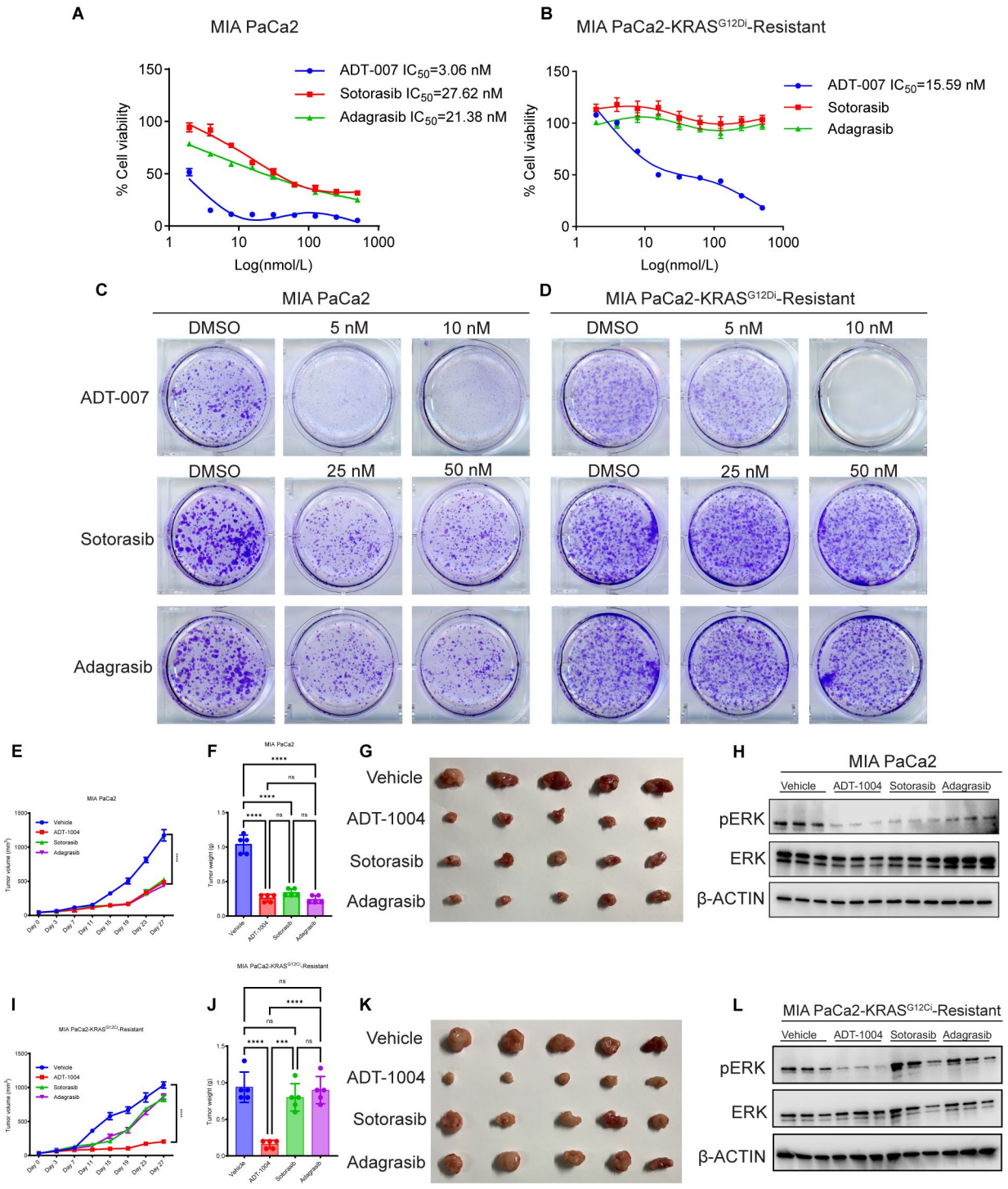

Figure 7: ADT-1004 demonstrates superior efficacy in suppressing the growth of KRAS^{G12Ci}-resistant cells compared to AMG-510 and MRTX849.

(**A-B**) PDAC cell lines were treated with different concentrations of ADT-007, sotorasib, and adagrasib for 3 days and analyzed for survival using the MTT assay. (**C-D**) Indicated PDAC cell lines were treated with the different concentrations of ADT-007, Sotorasib or Adagrasib for 2

898 weeks. Cell survival was then measured using clonogenic assays. Representative images are
899 shown. (**E** and **I**) MIA PaCa-2 or MIA-AMG-Res cells were injected subcutaneously into the
900 flanks of NSG mice (n=5). The mice were treated with either vehicle or ADT-1004, Sotorasib or
901 Adagrasib (40 mg/Kg body weight) orally, 5 days/week for 4 weeks. The average tumor volumes
902 over the course of the experiments are plotted. (**F** and **J**) Tumor weights were measured from
903 mice in the vehicle ADT-1004, sotorasib, and adagrasib (40 mg/kg) groups at the end of the
904 experiment under the indicated conditions for experiments in (**E** and **I**). (**G** and **K**)
905 Representative tumor images of NSG mice in the vehicle, ADT-1004, Sotorasib, and Adagrasib
906 (40 mg/kg) groups at the end of the experiment. (**H** and **L**) The indicated tumor tissues were
907 probed for pERK and total ERK expression by immunoblotting. β-Actin was used as a loading
908 control. Data represent the mean ± SEM. ns: not significant, *$p < 0.05$, **$p < 0.01$, ***$p < 0.001$,
909 and ****$p < 0.0001$.